Tampere University

Dharmendra Kumar Sharma

APPLICATION OF MACHINE LEARNING METHODS FOR HUMAN GAIT ANALYSIS

Master of Science thesis

Examiners: Prof. Robert Piché (TAU)
Dr. Pavel Davidson (TAU)

Master of Science Thesis
Examiners and topic approved on 26 September 2018

ABSTRACT

Dharmendra Kumar Sharma: Application of Machine Learning Methods for Human Gait Analysis
Master of Science thesis, 55 pages, 0 Appendix pages
Tampere University
Degree Programme in Automation Engineering, MSc (Tech)
August 2019

The majority of human gait analysis methods are limited to clinical gait laboratories. The calculation of gait parameters for athletes, during running in open environment, has endless possibilities of performance analysis to keep track of training. This thesis demonstrates a method to capture three-dimensional measurements of multidimensional human body movements during walking and running by means of GPS-aided-INS equipped data logger and also describes the two-dimensional (forward and vertical) analysis of captured three-dimensional movement.

The gait segmentation based on the vertical velocity has been presented and the built data processing software can compute majority of traditional gait metrics such as stride duration, average speed, stride length, cadence and vertical oscillation. The equipment uses inexpensive pressure insoles to generate foot pressure data for model training and indirect estimation of vertical ground reaction force and ground contact time. Both machine and deep learning approaches are detailed for indirect estimation of vertical ground reaction force and ground contact time. The possibilities are also explored to make interpersonal gait parameter estimation by means of generalised prediction models. Both machine leaning and deep learning solution are presented to generate continuous vertical ground reaction force curves along with gait components.

The methods, presented in this thesis, help to analyse human motion by means of gait segmentation and to calculate or estimate numerous spatio-temporal gait parameters. The intra-step variations in motion parameters are great help to analyse the different aspects of running in outdoor. The encouraging results reported in this thesis demonstrate the feasibility of device that provides detailed analysis about the performance of an athlete in outdoor running environment.

Keywords: Human gait analysis, ground reaction force, ground contact time, outdoor walking/ running, machine learning, deep learning, INS/GPS.

PREFACE

I planned my M.Sc. studies in Automation Engineering at Tampere University of Technology, back in 2017, which indeed was the biggest decision of my life. After two academic semesters, I have joined Position Algorithms Group at the Laboratory of Automation and Hydraulic engineering, in summer 2018, for data processing and app-design for OpenKin project. Machine learning and deep learning were completely new fields for me. Along with the app-design, I have also tried few state-of-the-art prediction techniques for vertical ground reaction force estimation. The initial prediction results during summer work were positive but not extraordinary due to my limited knowledge of the field at that time.

I would like to thank my thesis supervisors Prof. Robert Piché and Dr. Pavel Davidson for believing in me and giving me this thesis writing opportunity after the summer work. Although, I was having second thoughts about the master's thesis topic, but it was my supervisor's confidence which convinced me that I can successfully complete my thesis by continuing to work on the same project. This thesis work turned out be a journey from being a newbie to a mediocre in the field of machine learning and deep learning. I am also certain that I will continue to grow my field knowledge in upcoming years. I specially want to thank Heikki Virekunnas for data logger hardware setup, walk-run tests and various discussions. My thanks to Siva Kannan for project work briefing in the beginning of summer work. In addition, it was the positive effect of weekly meetings that I didn't lost the track and motivation for the work despite some setbacks.

I also wish to express my gratitude towards the funding agency, Academy of Finland, for the financial support to consortium "OpenKin: Sensor fusion for kinesiology research", grant 287295. The discussions, with the project collaborators at University of Jyväskylä, were also very informative for domain knowledge in human kinesiology. I am grateful to the automation engineering faculty and university services for their timely guidance and help which made this entire M.Sc. journey easier. I can't thank enough to my parents and siblings who believed in my dream of M.Sc. studies and friends, both in Finland and India, who were always there to support.

Tampere, 25 Aug. 2019

Dharmendra Kumar Sharma

CONTENTS

LIST OF FIGURES

LIST OF TABLES

LIST OF SYMBOLS AND ABBREVIATIONS

Abbreviations

2D	Two Dimensional
3D	Three Dimensional
4G	Fourth generation of broadband cellular network technology
AHRS	Attitude and Heading Reference System
BW	Body Weight
CoM	Center of Mass
GCT	Ground Contact Time
GCTL	Ground Contact Time of Left foot
GCTR	Ground Contact Time of Right foot
GCTs	both GCTL and GCTR
GNSS	Global Navigation Satellite System
GPS	Global Positioning System
GPU	Graphics Processing Unit
GRF	3D Ground Reaction Force
GRFL	3D Left Foot Ground Reaction Force
GRFR	3D Right Foot Ground Reaction Force
GRU	Gated Recurrent Units
HS	Heel Strike
IC	Initial Contact (or Touch Down)
IMU	Inertial Measurement Unit
INS	Inertial Navigation System
INS/GPS	GPS-aided Inertial Navigation System
Impulse_L	left foot impulse during the stride
Impulse_R	right foot impulse during the stride
kNN	k-Nearest Neighbour
LS	Least Square
LSTM	Long Short-Term Memory
NN	Neural Network
NRMSE	Normalised Root Mean Square Error
ReLU	Rectified Linear Unit
RMS	Root Mean Square
RMSE	Root Mean Square Error
RNN	Recurrent Neural Network
RP	Recursive Partitioning
RTK	Real Time Kinematics
TAU	Tampere University
TD	Touch Down
TDL	Touch-down event of left foot
TDR	Touch-down event of right foot
TO	Toe-off
TOL	Toe-off event of left foot
TOR	Toe-off event of right foot
UART	Universal Asynchronous Receiver-Transmitter
vGRFL	Vertical Ground Reaction Force of left foot
vGRFL_peak	Maximum vGRFL during the step/ stride
vGRFR	Vertical Ground Reaction Force of right foot
vGRFR_peak	Maximum vGRFR during the step/ stride
vGRFs	both vGRFL and vGRFR

Symbols

A_x, A_y, and A_z	3D accelerations in $x, y, \text{and } z$ sensor frame axis respectively
A_n, A_e, and A_d	3D accelerations in north, east and down geographical frame axis
A_f, A_s, and A_u	3D accelerations in anatomical (body) frame (forward, side and upward direction of motion)
b_i	are trainable bias vectors for layer i
B_i	i^{th} bag in ensemble
BW_i	body weight of i^{th} subject
c_t	LSTM cell state at time t
D	training data, $\{\langle x_i, y_i \rangle\}_1^n$
D_i	i^{th} disjoint partition of the training data
f_θ	a nonlinear function parametrized by θ.
f_t	LSTM cell forget gate output at time t
g	gravity vector
i_t	LSTM cell input gate output at time t
l	total number of disjoint partitions of D
M	the total number of decision trees in ensemble
n	total number of observations in training dataset D
o_t	LSTM cell output-gate's output at time t
O_v	vertical oscillation calculated from data logger
q_o, q_1, q_2, q_3	4D quaternions
$\Re$	rotation matrix
t	time point t
V_d	velocity by INS/GPS in downward direction in geographical frame
V_e	velocity by INS/GPS in geographical east
V_e^{gps}	velocity in geo-east measured by only-GPS, no sensor fusion
V_f	velocity in forward direction by INS/GPS (speed)
V_f^{gps}	velocity in forward direction measured by only-GPS
V_n	velocity in geographical north by INS/GPS
V_n^{gps}	velocity in geo-north measured by only-GPS, no sensor fusion
V_v	body velocity in vertical upward direction
ω_x, ω_y, and ω_z	3D angular velocities around $x, y, \text{and } z$ sensor frame axis
W_{ab}	trainable weight matrices for data from layer a to b
x_i	an input data feature in D
<x_i, y_i>	a datapoint in dataset D
y_i	a target output point in D
$\psi, \theta, \varphi, \theta_f^n$	yaw, pitch, roll and ground track
$\tilde{\psi}$, $\tilde{\theta}$, $\tilde{\varphi}$, $\widetilde{\theta_f^n}$	oscillations in yaw, pitch, roll and ground track (high pass filtered)
ϕ	empty set

1. INTRODUCTION

Walking is liberty. It is a simple activity for the majority of human population. Furthermore, for thousands of years, running has been the most prominent way to survival for human beings wherein in the modern world; it is a prerequisite to play several competitive sports.

Locomotion is a common and complex activity performed by people and normal walking/ running is a shared trait of healthy human beings. In medical terminology, the manner of human motion is termed gait whereas the detailed study of gait characteristics and gait abnormalities known as gait analysis. Humans are bi-pedal having two lower extremities and according to Nutt et al. [1], walking is synchronized movement of lower extremities with spanned flexion-extension in an involuntary and recurring fashion. Precisely speaking, gait is a combination of a cyclic pattern of locomotion and body posture. Although the domain experts prefer the use of word ‘gait’ rather than ‘walking’ but, both words are used interchangeably in the literature.

Humans have a distinguishable gait pattern because human beings are physically different from each other for the reasons of genetics, upbringing, and level of outdoor activities. Furthermore, age, personal energy level, neurological disorders, and mood are independent factors that have an effect on the gait characteristics. Undeniably, physical abnormalities and injuries are the major contributors to a dysfunctional gait pattern. The gait pattern comparison between feet is a traditional way to detect gait abnormalities. Finally, continuous gait parameter assessment measures efficiency in running and stability maintained during each step.

Humans can walk with an inefficient gait pattern for years without experiencing any discomfort. Besides, in the long term, an inappropriate way of walking can also result in permanent distortion in the gait cycle. A largely distorted gait resulting in health problems has enormous effects in daily life. In addition, an inefficient gait pattern has a negative impact on the performance of athletes in various sports. Therefore, precise gait pattern analysis, as well as its correction, is important. A thorough analysis of human motion is an area of interest for orthopaedists, physiotherapists, coaches, and researchers.

Over the years, numerous studies have been conducted to understand the gait cycle and now these studies are accommodating to numerous applications in different domains.

For instance, gait analysis for medical rehabilitation [2], animated games for rehabilitation [3], health and wellness gadgets [4], security [5], humanoid robotics [6], [7], and sports science [8] are a few examples of the human gait research and their applications.

Vision-based and sensor-based are traditional subjective methods for the gait parameter evaluation. Human gait analysis is already a challenging problem due to variations in human appearance and movement. Therefore, different methods are required as per application domain requirements and their accuracy obligations. In the later literature review, various methods for gait component estimation and their compatibility with outdoor motion analysis are detailed.

1.1 Vision Based Methods

In vision-based technologies, marker-based optical tracking techniques are widely used for the human gait and kinematics analysis (Wang et al. [9], Lee et al. [10], Prakash et al. [11]). In marker-based approaches, active (light emitting) or passive (reflecting) markers are attached to the body.

Figure 1. *Vision-based running gait analysis (an injury clinic, source [12])*

The subject has to walk through the area scanned by the instrumented camera system, an example shown in Figure 1. Thereafter, precise detection of markers is done by means of video analysis. The accuracy of the marker-based video analysis system, which can be up to ~1mm in order to locate an individual marker, is higher than markerless techniques. For sophisticated tracking systems 4-8 cameras, with frame-rate up to 300 fps [13], are used. For example, Vicon's camera system [14] is a pioneer in vision-based gait analysis and rehabilitation. It has fully automated marker labelling and tracking. By using this technique, the center of each marker can be recorded with sub-milli-

meter accuracy. Though these optical analysis technologies are precise but, their implementation requirements make them unsuitable for outdoor applications because of the following reasons:

- Expensive and bulky hardware.
- Need of trained personnel.
- Limited outdoor operability.
- Losing track of marker during video analysis [15].
- Inability to compute ground reaction force (GRF).

1.2 Sensor Based Methods

Sensor-based techniques for gait analysis provide an alternative to video-based methods. These techniques use two types of sensors i.e. body mounted sensors and force sensors. The body-mounted sensor includes inertial measurement units (IMU), Accelerometers or IMU combined with global positioning system (GPS) and the force sensor are mainly force plates or foot insoles. Force plates are ideal for kinetics calculations of human motion.

1.2.1 Inertial sensors

Inertial measurement units are a combination of accelerometers, gyroscopes, and sometimes magnetometers. An IMU measures linear accelerations (by using accelerometers), angular rates (by using gyroscopes) and heading (by using magnetometer). The orientation (yaw, roll and pitch) measurement system is an attitude and heading reference system (AHRS) which uses magnetometer for yaw angle and additional gravity vector for pitch and roll calculations. In addition, an inertial navigation system (INS) is a system (IMU + software) that can measure accelerations, angular rates, orientations along with continuous calculations of position (dead reckoning) and velocity (speed and direction) without any external reference.

Moreover, accelerometers and gyroscopes are attractive for gait analysis because they provide encouraging results for motion analysis [16]–[19]. This technology can be applied to measurement of spatio-temporal features such as velocity, displacement, angular rotation, cadence and stride-duration during the outdoor motion tracking [16], speed classification and gait stride calculation [17], and type of foot landing (rear-foot or fore/mid-

foot) [18]. Moreover, single or multiple IMU units are able to estimate basic spatio-temporal gait parameters when mounted on different parts of body [19], [20].

The following literature review shows that many investigators have tried multiple combinations of the IMU units and their placement on different parts of the human body. It includes IMU/ accelerometers mounted on foot [21], thigh [22], and waist [23], or multiple sensors on foot, shank and thigh [24]. The developed ambulatory monitoring systems in these publications can acquire information of multiple spatio-temporal gait parameters, e.g. speed, vertical displacement and gait events such as touch-down, toe-off, and heel-off. In addition, ground contact events (the type of foot strike, touch-down, and toe-off) are easier to detect [25], [26], by using algorithms with inertial sensor data, by means of slope/ peak features present in the data. In addition, the angular kinematics i.e. joint angles (e.g. knee, hip, and ankle) can also be determined by using multiple IMUs [27]. All in all, the use of multisensory IMU only systems for gait parameter calculation, is not viable because of

- dependence of acquired data on sensor orientation.
- lack of a single approach to calculate all parameters.
- inaccuracy of speed calculation due to integration error.
- unreliability of wireless data transmission in a multisensor system.
- inability to compute GRF.

1.2.2 Force platforms

Ground reaction force (GRF) is an important parameter of human motion analysis and it is the reaction force exerted by surface during motion. It is exerted on the feet, instead of the body's center of mass (CoM). Vertical GRF (vGRF) is non-propulsive type force meaning that it only restricts vertical body movement and has no effect on motion in forward direction. Force platforms are 'gold standard' for gait measurements but designed for use in indoor laboratories. Therefore, the challenge is to determine ground reaction forces and ground contact time in outdoor.

In medical technology, the combination of video and force platforms is a commonly used method in a dysfunctional gait assessment and rehabilitation. State-of-the-art force platforms, e.g. Strideway from Tekscan [2], have very high up to 500 Hz sampling rate for important gait parameters such as force, plantar pressure, temporal (time related), spa-

tial (distance related), and kinetic (joint movement) features. This system has the capability of synchronization with optical systems and provide a convenient graphical user interface. In addition, this system supports gait assessment needs for clinical purposes such as symmetry and difference gait parameter tables for left and right foot comparison [2]. The drawbacks of these tools to outdoor operability include

- limited portability and small area covered.
- the need for a trained operator for test and analysis.
- the need for floor integration i.e. the force plat should be at the same level as floor.
- the need for synchronization among multiple force-plates and video systems.

Briefly, six-dimensional force platforms, when used with optical tracking systems, are clinically accepted 'gold standard' for gait evaluation. These technologies are widely accepted when the experiments are restricted to a few continuous steps of walking and running in a laboratory environment. In conclusion, it is safe to claim that vision-based approaches and force platforms are not feasible for outdoor motion acquisition and analysis for a large number of footsteps.

1.2.3 Instrumented foot insoles

Instrumented insoles are an alternative to force platforms. Unlike force platforms, instrumented insoles can be used everywhere (not only in specially equipped labs). They do not impede the athlete's natural movements. However, they are not as accurate as force platforms. Over the years, different types of instrumented foot insoles have been developed [28]–[31]. These instrumented insoles either have an on-board data storage or real-time data logging [32]. Interestingly, the instrumented insoles can function similar to the force plates, but their accuracy depends on the type of the pressure sensor (capacitive or piezo-resistive) used and their design specifications. Precisely speaking, the instrumented insoles are only an approximate alternative to force plates since insole measurements are not very accurate when compared with the force platform, especially vGRF curve peaks do not match [33], [34]. Consequently, vGRF measurements by foot insoles might require scaling or calibration to match the force plate's measurements. In addition, the insoles measure a single component of GRF i.e. vGRF, unlike 3D GRF measurement by using force platforms. The foot insoles are suitable to use for gait assessment during walking and running in outdoor but have following downsides

- Dependence on shoe-size.
- Need of frequent calibration (pressure zeroing).
- Short life and damage possible due to running on rough surface [35].
- Inaccuracy when compared with force platforms.

1.2.4 Integrated INS/GNSS systems

Satellite navigation and inertial sensors are widely used for motion tracking and biomechanics research. The high accuracy GNSS receivers are used to determine the position and average speed during the gait cycle. The speed acquired from GNSS has low time resolution due to a low data rate of GNSS devices. Consumer grade GNSS receivers have a data update rate of 1-5 Hz whereas the GNSS receivers with embedded RTK (real time kinematics) functionality provides an output rate up to 20 Hz with centimeter-level accuracy in position measurement [36]. Although, an INS measures accelerations and in addition, by processing the acceleration data, a single integration of 'short duration' acceleration data provides velocity and double integration provides displacement, during 'long-term' INS suffers from accumulated integration error ("drift") in position and velocity calculations.

GPS-aided Inertial Navigation Systems (INS/GPS) combine an advanced global positioning system (GPS/GNSS) receiver with INS sensor and outputs position, velocity, and attitude estimates [37]. There are several methods for GPS and INS data integration/ fusion [38]. After fusion corrections, 3D-velocity vectors contain precise intra-stride variations [39], [40]. The precise velocity measurement is very important for runners and athletes since it helps to understand their running style. The intra-stride variations of INS/GPS data parameters can help to explain the pattern of vGRF curves. In addition, the precise details of measured 3D velocity make it possible to calculate the vertical distance (by using vertical velocity) and stride length (by using forward velocity). This high accuracy of speed measurements is backbone of gait segmentation technique. Moreover, ready to use GPS-aided-INS sensors are also available, e.g. VN200 from VECTORNAV [37], and they can provide speed accuracy up to ±0.05 m/s with an INS output data rate of 800 Hz, navigation data rate of 400 Hz and GNSS correction rate of 5 Hz.

1.2.5 Indirect methods

It is also possible to eliminate the need of force platforms and instrumented insoles by indirect estimation of vGRF and ground contact time (GCT) if their correlation with INS/GPS data parameters is well understood. Besides, there is always a requirement of force sensors for training data collection. The correlation between temporal and spatial gait features has already been discussed in several articles. For example, the negative correlation between GCT and speed is well known and easy to comprehend [41]. The trend of the vGRF with speed (for walking, slow-jogging, jogging, and running), body weight (BW) and gender has been discussed by Keller et al. [42]. In addition, the shape of vGRF curve depends on the type of foot strike [42]. Moreover, the correlation of walking speed with stride length, cadence, and stride time is presented by Tanawongsuwan et al. [43] whereas a thorough analysis of the relationship of speed with GCT (also known as stance time), foot-strike, peak vGRF, vGRF curve shape, and impulse has been demonstrated by Tongen and Wunderlich [44].

Furthermore, if vGRF curve and GCT labels of both feet are estimated with enough accuracy then single support, double support and flight time can also be determined. The vGRF is highly correlated with movement of the body's CoM in vertical direction (i.e. vertical- acceleration, velocity and displacement) therefore there were some attempts to predict vGRF by using uniaxial IMU data. For example, prediction of vGRF for human walking and running using a foot mounted uniaxial accelerometer with the neural network (NN) has been demonstrated by Ngoh et al. [45]. They claim this approach to be the first application of NN and uniaxial accelerometer for vGRF estimation during running. By using uniaxial accelerometer data, it also reduces the requirement of using multiple wearable body sensors and the use of NN minimizes the computational necessity for vGRF prediction. Similarly, the use of single IMU (sacrum mounted) based 3D-GRF estimation has been shown by Gurchiek [46] by using the Bland-Altman analysis.

Recent advances in consumer grade electronics have pushed the use of numerous activity trackers but these devices are limited in use, for example- step count, heart rate, and energy expenditure estimation [47], [48]. Advanced fitness trackers [49] can also estimate a few dynamic parameters such as- cadence, vertical oscillation, GCT and stride length but the technology used is a trade secret.

Finally, in recent articles, the more advanced and sophisticated indirect methods usually use convolution neural network [50] or artificial neural network [45], [51], [52] to compute relationships between the acceleration vectors and gait features. Besides GRF, indirect

measurements of GCT and gait events (heel-strike and toe-off) [53] and 100% gait phase (Initial contact, mid mid-stance, terminal mid-stance, push off, pre-swing, initial swing, mid swing and terminal swing) prediction [54] has also been demonstrated in scientific publications. The indirect methods require a large amount of training data to make a prediction. However, due to physiological difference, universal (person independent) vGRF/ GCT prediction model development is still an open question.

1.3 The approach taken in this work

In the previous sections of this literature survey, different gait assessment techniques and gait parameter evaluation setups (devices) have been discussed keeping their outdoor usability in mind. There is a strong need of a device that can measure and predict majority of gait components (both temporal and spatial) during outdoor walking or running, without compromising the natural movement of the subject.

This work uses the single body-mounted data logger that has been developed at Tampere University under the project “OpenKin- Sensor Fusion for Human Kinesiology” [55]. It helps to get rid of the need for multiple body-worn sensors and acquires 3D linear velocities, 3D linear accelerations, 3D angular rates, and orientations at the output data rate of 400 Hz. In addition, Moticon foot instrumented insoles are used to acquire foot pressure data. As shown in Figure 2, the aim of this thesis is to develop a vertical velocity-based gait segmentation technique to acquire gait metrics and, to show indirect techniques for vGRF and GCT estimation by taking INS/GPS data as input and to train prediction models with the help of target data acquired from Moticon insoles.

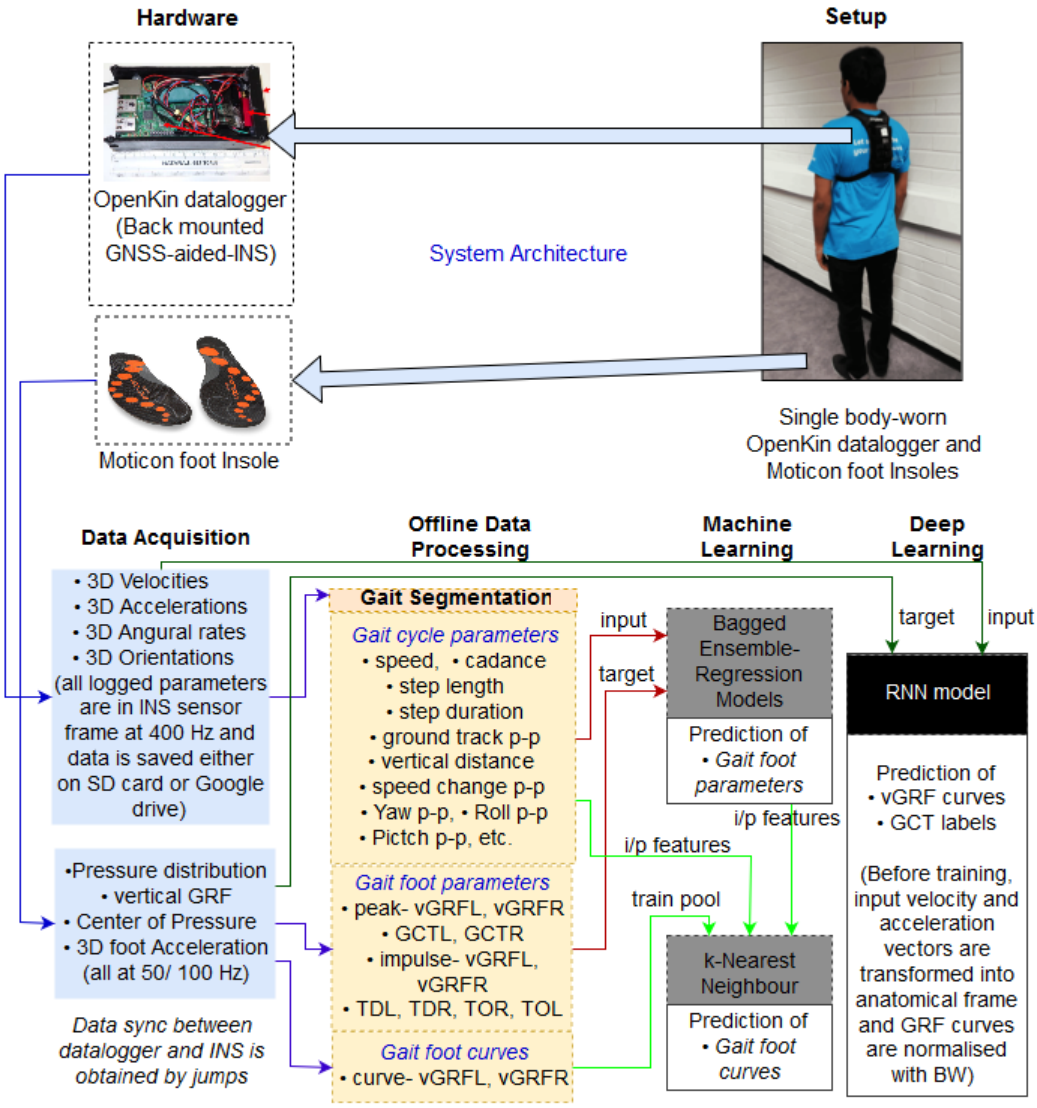

Figure 2. *System Architecture*

1.4 The roadmap of this thesis

In the later sections of this thesis, Section 2 describes the basics of human gait analysis and machine learning techniques applied for this thesis work. Further, details of the INS/GPS data logger and Moticon insoles are given in Section 3 along with gait segmentation method and running metrics components. Further, section 3.6 illustrates the details of logged datasets along with procedure for field tests and offline data processing. Indirect measurements methods of GCT and vGRF, namely machine learning and deep learning, are detailed in section 4.1 and 4.2, respectively, with thorough discussions on problem solving approach and obtained results. Conclusion and Future work are in Section 5 and 6 respectively.

2. PRELIMINARIES

2.1 Basics of Human Gait

The gait cycle is a sequence of foot events that repeats cyclically during locomotion. It is also referred as gait stride and can be defined with reference to either foot. It begins with initial foot contact to the surface (Touch-down, TD) and ends at the subsequent Touch-down of the same foot. In addition, a gait stride consists of a complete footstep of the reference foot and also a full or incomplete (depending on locomotion speed) footstep of the other foot. Moreover, during the gait cycle the body CoM is propelled in forward direction and the distance travelled during one gait cycle is called stride length.

2.1.1 Gait cycle

A pictorial representation of the gait cycle (considering the right foot as reference) is shown in Figure 3. Broadly, a gait cycle can be divided into two phases i.e. stance-phase and swing-phase.

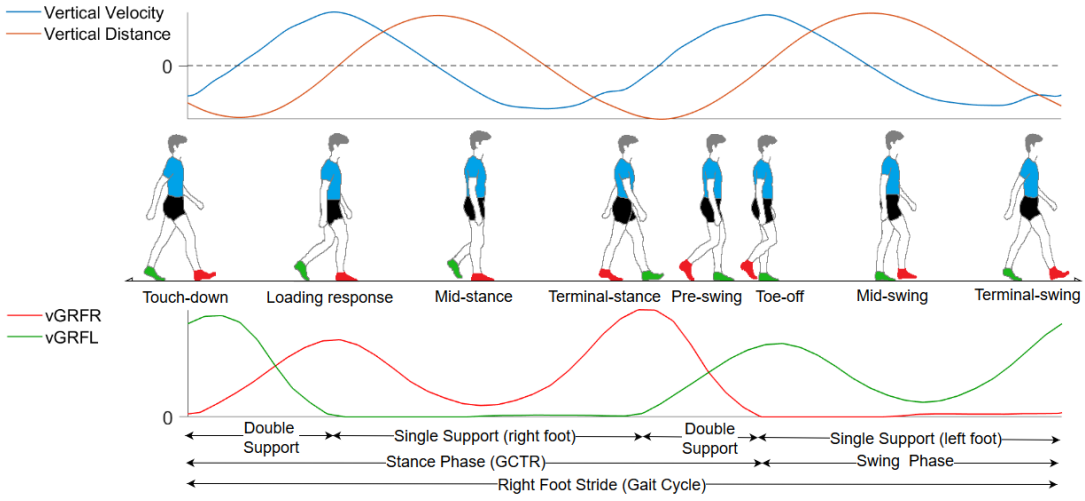

Figure 3. *Gait cycle; synchronized vGRFs (from Moticon insoles) and vertical CoM motion (from INS/GPS) at walking speed of 1.72 m/s*

The stance phase (also known as GCT) is the time duration in the gait cycle when the foot remains in contact with the surface, starting with Touch-down and ending at Toe-off (TO). Subsequently, the swing phase starts with TO and lasts until the end of the gait cycle i.e. next TD. Therefore, the swing phase is when the foot is in motion and not touching the ground surface. For normal walking, nearly 60% of the gait cycle is stance

phase when foot is bearing the weight of body and the swing phase is the remaining 40% [56], [57]. It is also possible to divide gait cycle into 2-8 phases, as per analysis requirements, by considering several gait-partitioning methods [58]. The gait cycle division into eight sub-phase or gait events, which are critical for gait abnormality analysis, are following:

Touch-down: This is the instant when the reference foot makes initial contact with the ground. It is also known as heel-strike (HS), but the use of TD is more correct since HS may not occur during running.

Loading Phase (also contact phase): This begins with TD of the reference foot and ends when both fore and rear part of reference foot start bearing the BW (soon after TO of other foot, [56]). In this phase, the vGRF reaches the braking force peak which is slightly greater than BW [56].

Mid-stance: The time interval when both forefoot and rearfoot is on the ground. The vGRF decreases below BW at middle of mid-stance [56].

Terminal-stance: This involves the propulsive vGRF and during this phase, the heel of the reference foot leaves the ground and vGRF is maximum at second peak that is also known as propulsive peak.

Pre-swing: This is the period of transition between stance and swing phase i.e. vGRF decreases and becomes zero after the TO.

Toe-off: The instant when the reference foot leaves the ground.

Mid-swing: The instant when the knee reaches its peak height and advancement of the limb continues.

Terminal-swing: The foot is in position of the next TD, and advancement of the shank continues.

Moreover, the above gait phase terminology is important if the gait segmentation method is foot contact based. This thesis presents a vertical velocity-based gait segmentation method (detailed in section 3) which takes account of the vertical movement of body CoM. During normal walking, the body CoM follows the “curate cycloid” motion which is similar to the arc of a circle [59]. The vertical velocity and vertical oscillation of CoM (measured by INS/GPS), in synchronisation with the gait cycle and vertical foot forces, have been shown in Figure 3.

A possible error source is the fact that the OpenKin data logger is mounted on the torso and not at CoM of body. However, the data logger is tightly mounted on torso, inside a well-fitting running-backpack-vest that allows the data logger to follow the position and orientation similar to body during locomotion. Therefore, the data logger's movement is similar as body CoM movement, which justifies the approximation that the data logger is fixed to the CoM of the body.

2.1.2 Gait terminology

The important gait terms with their definition are enlisted in Table 1.

Table 1. Gait Terminology

Term	Definition
Normal Gait	A gait cycle without any major dysfunction [60]
Gait Phase	A specific duration in gait cycle
Gait Event	A specific instance in gait cycle
Gait Segmentation	A process to divide continuous motion into gait strides
Stride/ Gait Stride	A complete gait cycle
Step	A complete foot-step (TD to TO) of reference foot
GRF	3D ground reaction forces
vGRF	Vertical component of GRF
Peak vGRF	Maximum vGRF during the step/ stride ('vGRFL_peak' for left foot and 'vGRFR_peak' for right foot)
Impulse	Area under vGRF curve during the stride (to quantify changing-vGRF over the GCT, 'Impulse_L' for left foot and 'Impulse_R' for right foot).
GCT	Total time in stride when foot is in contact with surface
Contact Label	'1' if foot is in contact with the surface, '0' otherwise
Braking Peak	vGRF peak during loading response (to absorb the shock)
Propulsive Peak	vGRF peak during terminal stance (to leave the ground)
Rearfoot Landing	When footstep start with heel-strike
Forefoot Landing	When footstep does not start with heel-strike (possible during running)

The gait parameters related to the distance (covered during movement) are termed as spatial gait parameters, described in Table 2.

Table 2. Spatial Gait Parameters

Parameter	Definition
Stride Length	Distance covered in motion direction during a gait stride
Step Length	Distance covered in motion direction during a step
Vertical Oscillation	Oscillatory motion of the body CoM in vertical direction
Vertical Distance	Peak-to-peak vertical oscillation during gait stride
Stride Width	Distance between left and right foot mark (perpendicular)
Center of Pressure	Centroid of vGRF during the step

The time dependent gait parameters, termed temporal gait parameters, are listed in Table 3.

Table 3. Temporal Gait Parameters

Parameter	Definition
Speed	Magnitude of forward velocity during gait stride
Cadence	Strides covered during motion per minute
Stride Duration	Gait cycle duration
Single Support	Time duration in gait cycle when single foot is bearing BW
Double Support	Time duration in gait cycle when both feet are bearing BW
Flight Time	Time duration in gait cycle when both feet are in air
GCTL	Time duration in gait cycle when left foot is in contact with surface
GCTR	Time duration in gait cycle when right foot in contact with surface
TOR	Right foot toe-off time (measured from start of gait cycle)
TDR	Right foot touch-down time (measured from start of gait)
TOL	Left foot toe-off time (measured from start of gait cycle)
TDL	Left foot touch-down time (measured from start of gait cycle)

Spatial and temporal parameters are related to the distance and time respectively. In addition, gait parameters, dependent on both distance and time, are also known as spatio-temporal or time-distance parameters. In human kinematics terminology, the kinetic gait parameters include joint angles, angular motion and angular rates.

2.1.3 Vertical ground reaction force

The vertical ground reaction force is the largest component of 3D GRF acting on the foot during footstep. The vGRF, in magnitude, is around 10 times larger than antero-posterior force (in x direction) and almost 100 times of medial-lateral force (in y direction) [44]. The coordinate assumptions for locomotion are, 'x' in forward (antero-posterior), 'y' in side (medial-lateral) and z in vertical direction. Left and right foot vGRF time-history for a gait stride is shown in Figure 3. For walking, vGRF has 'M' shape curve (first shown in 1872 by G. Carlet in PhD thesis [61]) and for running, it is of inverted 'V' shape. In addition, the peak vGRF is comparable to BW during the walking [62] and higher than BW during the running. Therefore, the large magnitude and the direction of vGRF makes it easier, among 3D GRF, to measure by placing the pressure sensors between foot and surface. Finally, it is also possible to detect foot contact label and further GCT by setting a threshold to vGRF since vGRF is non-zero when the foot is in contact with the surface.

2.2 Machine Learning Methods Used

Machine learning algorithms are complex statistical fitting methods applied to large data sets. For learning and prediction, classical machine learning methods use attributes extracted from data vectors by using feature extraction methods whereas in deep leaning feature extraction is automated. Following is a brief description of the machine learning methods used in this thesis work.

2.2.1 Regression trees and bagged ensembles

Decision trees, in general, are human-interpretable-logic based machine learning algorithms and are used for both regression (called regression trees) and classification problems.

A regression tree method based on least squares (LS) was first introduced by Breiman et al. in 1984 [63] as classification and regression tree (CART) method. The regression tree splits the data into smaller subgroups and then assigns a constant value for every observation in that subgroup. Formally speaking, a regression tree can be described as an additive model, as per Hastie & Tibshirani [64], of the piecewise constant regression models which divides the dataset (D) to multiple regions (D_i) and fit a constant value model (k_i) in each region [65].

$$m(x) = \sum_{i=1}^{l} k_i \times I(x \in D_i) \tag{2.1}$$

Here k_i are constants;

- $I(.)$ is an indicator function returning 1 if its argument is true and 0 otherwise;
- D_i are disjoint partitions of the training data, $D = \{\langle x_i, y_i \rangle\}_1^n$, such that $\bigcup_{i=1}^{l} D_i = D$ and $\bigcap_{i=1}^{l} D_i = \phi$. Here, n is total number of observations in dataset D.

The splitting of predictor space x is done at a node (represents a feature, x_i) leading towards the leaves (value outcomes) via the branch links (decision rules). The total number of disjoint partitions (l) is equal to the number of leaf nodes in the tree, therefore, each leaf node holds the prediction value of corresponding partition.

In a basic regression tree, the partitioning at nodes is obtained by successive binary partitioning by a set of rules. The "Successive Binary Partition" or "Recursive Partitioning (RP)" is a greedy algorithm that recursively splits dataset into two subsets and tries to minimise the cost of splitting. The simplest way of building a regression model in RP is to minimise the LS error (cost of splitting) in which the predicted outcome is the mean of the spited dataset

$$\frac{1}{n}\sum_i^n \big(y_i - r(\beta, x_i)\big)^2 \tag{2.2}$$

- Here, n is the sample size;
- $<x_i, y_i>$ is a data point;
- and $\mathrm{r}(\beta, x_i)$ is the prediction of the regression model $\mathrm{r}(\beta, x)$ for the case $\langle x_i, y_i \rangle$.

The RP algorithm is computationally expensive due to the necessity to find the best split for each node. To overcome such problems several split approaches, such as arbitrary split can be used. Another method is 'least absolute deviation' which results into having median of the partition at leaves instead of mean [65].

Unfortunately, due to high variance, a regression tree is a poor predictor for complex regression problems and tends to overfit. However, the bagged ensemble [66] improves generalisation and reduces overfitting by combining (average for regression and voting in case of classification) several bootstrap aggregated decision tree results. The bagged ensemble method works well when the prediction models have low bias but high variance [67], such as decision tree with large depth. The variance reduction is maximum when the bootstrap samples, used to generate decision trees, are independent [66]. The decision trees are built deep enough, with enough leaf size, to have low bias. Moreover, variance can be reduced up to factor M by considering bagged ensemble. Here, M is the number of decision trees in ensemble. There are not much theoretical results in literature

about the reduction in variance of bagged ensembles since it depends on the independence of the bootstrap samples. The bagged ensembles in Figure 4 can be explained as following:

- Bootstrap sampled M sub-datasets are created with each having sample size m.
- A single regression tree is trained for each sample and average of all M prediction model from every tree is calculated.
-

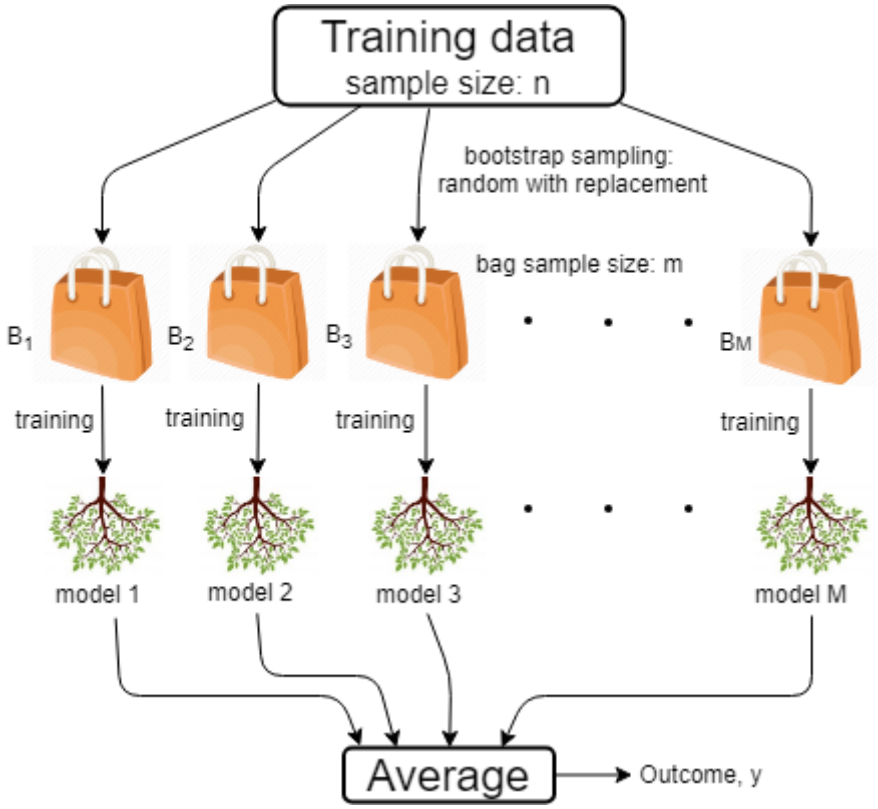

Figure 4. *Bagged ensemble of regression trees*

Random forests are next level to the bagged trees to have better prediction by further randomizing the data by the feature sub-sampling for each node split. Random forest algorithms outperform bagged trees significantly only if there are many input features available which is not our case after optimal feature selection is done.

2.2.2 k-nearest neighbor (kNN)

Nearest neighbor based machine learning algorithms are used for both unsupervised and supervised problems. Normally, unsupervised nearest neighbour methods are used for clustering problems whereas supervised nearest neighbour methods are used for both classification of discrete labelled data, and regression for continuous labelled data. The main idea behind the nearest neighbour algorithms it to determine the predefined

index of training samples, nearest in distance to the new test point and predict the label from chosen nearest samples [68]. Being a simple and non-parametric method, it is often successful in classification situations where the decision boundary is very irregular. The number 'k' (kNN learning) is often user defined. The decision parameter is distance (of k minimum) and standard euclidean distance is common choice for it. The nearest neighbour methods are computationally expensive because they are required to remember the complete training dataset in order to make a prediction therefore, they are non-generalised methods. Finally, if the features in kNN feature space have uniform weight then they are equally important and have same dimensions.

2.2.3 RNN and LSTM

Sequence learning is unique among supervised learning problems because sequence is a well-defined order of observations. This order of the data sequence, which defines the collective meaning of the sequence, must be unaltered [69] during model training and prediction generation. Preceding elements are the basis of the prediction of the next element in the sequence [70]. The architecture of recurrent neural network can be imagined as the addition of loops to standard feedforward multilayer perceptron (MLP) network. However, MLP can only map input data vector to the target data vector whereas, the RNN, in theory, are able to map the entire target data vectors from the history of previous data inputs. In RNN, it is possible for a neuron to pass a signal laterally (sideways in same layer) in addition to forward to the next layer. Sometimes, the feedback (of output) with next input vector is also possible to feed as input to the network. The RNN connections adds a state (allows them to learn) and a memory (helps to understand the ordered and sequential nature of the observations in input) to the network. For supervised problems, the RNN can be trained by backpropagation through time. However, the RNN may not be able to learn the long sequence dependencies due to the vanishing gradient problem.

The Long Short-Term Memory (LSTM) network is a special type of RNN that avoids the vanishing gradient problem during training and is designed to learn long-range data dependencies. The LSTM mathematics in taken from the deep learning survey published by Jianqing Fan et al. [71].

Suppose our time series sequence inputs are $x_1, x_2, \ldots, x_T$. The recursive formula for a basic RNN that models the hidden state at time t by vector h_t

$$h_t = f_\theta(h_{t-1}, x_t) \tag{2.3}$$

Here, f_θ is generally a nonlinear function parametrized by θ.

Concretely, a basic RNN with one hidden layer with the *tanh* activation

$$h_t = tanh(W_{hh}h_{t-1} + W_{xh}x_t + b_h) \tag{2.4}$$

$$y_t = \sigma(W_{hy}h_t + b_y) \tag{2.5}$$

Here, $W_{hh}, W_{xh}, \text{and } W_{hy}$ are trainable weight matrices, $b_h \text{ and } b_y$ are trainable bias vectors, and y_t is the output at time t.

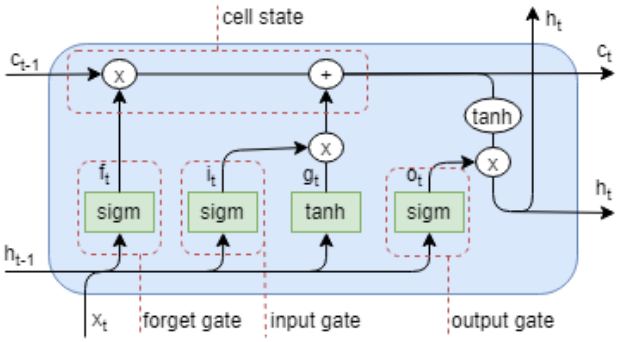

Figure 5. *LSTM Cell*

The computational unit of the LSTM network is called the cell or memory cell. LSTM cells are comprised of weights and gates. A memory cell has weight parameters for the input, output, as well as an internal state that is built up through exposure to input time steps.

The existing gates in the LSTM is what distinguishes it from basic RNN networks. These gates are the weighted functions that allow or restrict the flow of the information in the cell. As shown in Figure 5, there are three gates in each LSTM cell. The forget gate and input gate are used in the updating of the internal state (also called cell state). The output gate decides actual output of the cell. It is these gates and the consistent data flow, called the constant error carrousel or CEC, that keep each cell stable (neither exploding nor vanishing).

The LSTM maintains a cell state c_t which is throughout the time depending on the present input. The functioning of the gates can be described as equation below, where element-wise multiplication is donated by $\odot$ and element wise sum is donated by (+).

$$\begin{bmatrix} i_t \\ f_t \\ o_t \\ g_t \end{bmatrix} = \begin{bmatrix} \sigma \\ \sigma \\ \sigma \\ tanh \end{bmatrix} \mathrm{W} \begin{bmatrix} h_{t-1} \\ x_t \\ 1 \end{bmatrix} \tag{2.6}$$

$$c_t = f_t \odot c_{t-1} + i_t \odot g_t \tag{2.7}$$

$$h_t = o_t \odot \tanh(c_t) \tag{2.8}$$

Here,

- W is a weight matrix with required dimensions.
- c_t is cell state vector and carries information of sequence.
- forget gate f_t decides the values of c_{t-1} to keep (remember) for time t.
- i_t is input gate which controls the update to the cell state.
- the output gate o_t gives how much c_t reveals to h_t. Ideally, the elements of these gates have nearly binary values. For example, an element of f_t being close to 1 may suggest the presence of a feature in the sequence data.
- Similar to the skip connections in residual nets, the cell state c_t has an additive recursive formula, which helps back-propagation and thus captures long range dependencies.

3. CONTINUOUS MONITORING OF HUMAN MOVEMENT

3.1 Device (OpenKin Data Logger)

The OpenKin data logger is made up of a Vectornav VN-200 INS/GPS connected to programmed Raspberry Pi 3 board, both powered by 4200 mAh power bank [55]. All these components are packed in a 3D-printed box. The INS/GPS data is acquired through UART by Raspberry Pi and stored on a memory card. A 4G/LTE USB modem is connected to Raspberry Pi and at the completion of the experiment the data, from memory card is uploaded to the cloud.

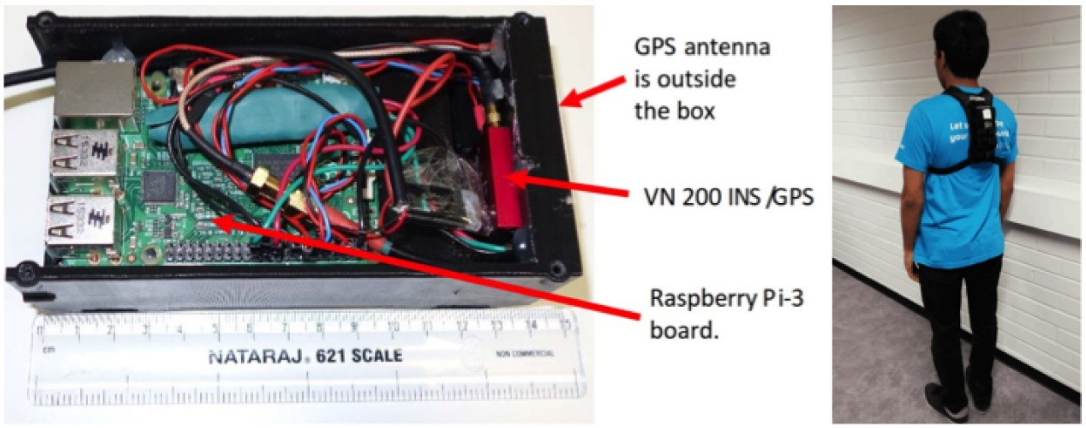

Figure 6. *OpenKin data logger hardware mounted on human back [55]*

This self-contained data logger has following properties [55].

Size and Weight: 150 × 75 × 48 mm^3, about 400 g,

Output rate: 400 Hz,

Expected single charge runtime: 5-6 h.

The VN-200 INS-aided-GPS sensor is the heart of the OpenKin data logger. The best accuracy of VN-200 data is achieved when GPS signal is free from multipath. It is a factory calibrated high accuracy sensor with the following specifications [37]:

Velocity accuracy: ±0.05 m/s,

Orientation accuracy: Pitch/Roll: 0.1° RMS and Heading, true inertial: 0.3° RMS

Angular resolution: <0.05°.

The data logger continuously logs the following parameters (metrics) at the rate of 400 Hz.

- **3D acceleration**: (A_x, A_y, and A_z), Here x, y and, z are axes of sensor frame,
- **4 Dimensional Attitude Quaternion**: (q_o, q_1, q_2, q_3), are components of quaternions in a specific order for VN-200 sensor [72],
- **3D Velocity from INS/GPS sensor fusion**: (V_n, V_e, and V_d), here n, e and, d are north, east, and down axes of geographical frame,
- **3D Angular Velocity**: (ω_x, ω_y, and ω_z), in sensor frame
- **2D GPS Velocity**: (V_n^{gps}, and V_e^{gps}), velocity measured by only GPS without any sensor fusion

The offline processing, by MATLAB software, is performed to acquire the following parameters

- **3D Orientation**: (yaw: ψ, pitch: θ, and roll: φ),

  The orientation angles are calculated by using quaternion mathematics [72].

$$\psi = atan\left(\frac{2(q_0 q_1 + q_2 q_3)}{{q_3}^2 - {q_2}^2 - {q_1}^2 + {q_0}^2}\right) \tag{3.1}$$

$$\theta = asin\left(-2(q_0 q_2 - q_1 q_3)\right) \tag{3.2}$$

$$\varphi = atan\left(\frac{2(q_1 q_2 + q_0 q_3)}{{q_3}^2 + {q_2}^2 - {q_1}^2 - {q_0}^2}\right) \tag{3.3}$$

- **3D Acceleration in geographical frame:** (A_n, A_e, and A_d), here n, e and, d are north, east, and downward axes of geographical frame,

$$\begin{bmatrix} A_n \\ A_e \\ A_d \end{bmatrix} = \mathfrak{R}^T \begin{bmatrix} A_x \\ A_y \\ A_z \end{bmatrix} \tag{3.4}$$

  Here, $\mathfrak{R}^T$ is transpose of $\mathfrak{R}$. The $\mathfrak{R}$ is a rotation matrix and $\psi, \theta, and\, \varphi$ are yaw, pitch and roll angles respectively i.e. orientation of the sensor frame axis with respect to geographical frame looking in counterclockwise direction.

$$\mathfrak{R} = \mathfrak{R}_z(\psi) \cdot \mathfrak{R}_y(\theta) \cdot \mathfrak{R}_x(\varphi) \tag{3.5}$$

$$\Re = \begin{bmatrix} \cos(\psi) & \sin(\psi) & 0 \\ -\sin(\psi) & \cos(\psi) & 0 \\ 0 & 0 & 1 \end{bmatrix} \cdot \begin{bmatrix} \cos(\theta) & 0 & -\sin(\theta) \\ 0 & 1 & 0 \\ \sin(\theta) & 0 & \cos(\theta) \end{bmatrix} \cdot \begin{bmatrix} 1 & 0 & 0 \\ 0 & \cos(\varphi) & \sin(\varphi) \\ 0 & -\sin(\varphi) & \cos(\varphi) \end{bmatrix} \tag{3.6}$$

- **Forward Speed**: (V_f), speed in the direction of the horizontal movement (calculated by INS/GPS fusion)

$$V_f = \sqrt{{V_n}^2 + {V_e}^2} \tag{3.7}$$

- **Forward GPS Speed**: (V_f^{gps}), speed in the direction of the horizontal movement (measured by only GPS)

$$V_f^{gps} = \sqrt{V_n^{gps} + V_e^{gps}} \tag{3.8}$$

- **Ground Track** (θ_f^n): it is the path of movement seen from above the ground i.e. direction of horizontal (forward) movement with respect to the geographical north.

$$\theta_f^n = \operatorname{atan}\left({V_e}/{V_n}\right) \tag{3.9}$$

V_f and θ_f^n, in combination, define forward velocity. The accuracy of ground track angle depends on the speed (V_f) of movement and is best when speed is greater than 1.5 m/s [55].

- **3D Acceleration in anatomical frame:** (A_f, A_s, and A_u), where, in these experiments the anatomical (body) frame for human movement is defined as f in forward, s in subjects' right hand side direction and u in vertically upward direction.

$$A_f = A_n \cos\left(\theta_f^n\right) + A_e \sin\left(\theta_f^n\right) \tag{3.10}$$

$$A_s = -A_n \sin\left(\theta_f^n\right) + A_e \cos\left(\theta_f^n\right) \tag{3.11}$$

$$A_u = -A_d - g, \tag{3.12}$$

Here, g is apparent gravitational acceleration.

- **Orientation oscillations**: ($\widetilde{\psi}$, $\tilde{\theta}$, $\widetilde{\varphi}$, $\widetilde{\theta_f^n}$), The true body oscillations can be accurately determined after removing drift from the yaw, roll, pitch and ground track vectors using the $highpass$ function of MATLAB's Signal Processing Toolbox. The function's input parameters are: Normalized passband frequency (wpass), 0.005 rad/sample; attenuation (stopbandattenuation), 30 dB; and steepness wpass (steepness), 0.7. The $highpass$ filter removes the drift in yaw due to change in direction, and in pitch due to inclination/ declination of the surface. The pseudo MATLAB code is following-

$$\begin{bmatrix} \widetilde{\psi} \\ \tilde{\theta} \\ \widetilde{\varphi} \\ \widetilde{\theta_f^n} \end{bmatrix} = \text{highpass}\left(\begin{bmatrix} \psi \\ \theta \\ \theta \\ \theta_f^n \end{bmatrix}, 0.005, '\text{ StopbandAttenuation}', 30, '\text{ Steepness}', 0.7 \right); \quad (3.13)$$

here, ψ, θ, φ and θ_f^n are row vectors.

- **Vertical Velocity**: (V_v), is the high pass filtered vertical component of the 3D velocity measured by INS/GPS and positive in the vertical upward direction. The pseudo MATLAB code of vertical velocity is following-

$$V_v = \text{highpass}(-V_d, 0.005, '\text{ StopbandAttenuation}', 30, '\text{ Steepness}', 0.7); \quad (3.14)$$

The high pass filter, in case of vertical velocity (see Figure 8 and 9), filters the low-frequency drift caused mainly by accelerometer bias and due to motion on an uneven track [55].

- **Vertical oscillation: (O_v)**, The vertical movement of the data logger (CoM) can be achieved by integration of $-\mathrm{V_d}$ (vertical component of the CoM's velocity considering positive in upward direction) over time. Thereafter, pure vertical oscillations can be derived by applying similar high pass filter, as in equation 3.14, on integrated $-\mathrm{V_d}$. Integration was implemented in MATLAB using trapezoidal integration by using function trapz [73] since data points are evenly spaced at 400Hz. The derived vertical oscillations explain the distance of the body CoM from the surface, as previously shown in Figure 9 and 10 of Davidson et al. [55]. The shape of the vertical oscillation curve also agrees with the curtate cycloid motion of the body CoM proposed by Carpentier et al. [59].

$$O_v = \text{highpass}(trapz(-V_d), 0.005, '\text{ StopbandAttenuation}', 30, '\text{ Steepness}', 0.7) \quad (3.15)$$

3.2 INS/GPS vs Only GPS

As mentioned in the previous section, with the help of VN-200 sensor in data logger, we can compute forward velocity by means of both INS/GPS and only GPS. Figure 5 and 6 in Davidson et al. [55] shows the forward velocities acquired using both methods. There are two clear advantages of using INS/GPS integrated sensor. First, the forward velocity logged by INS/GPS at 400Hz therefore it contains intra-stride details. Second, the accuracy of the only GPS is not very accurate when signal is poor due to multipath errors and the data logging rate is only 5Hz. Therefore, INS/GPS informs us about acceleration and deceleration that happened during the stride.

3.3 Moticon Insoles

Moticon wireless sensor insoles logs the pressure of 13 capacitive pressure sensors per sensor insole. The 13 sensors cover ~50 % of insole surface [74], and have pressure range of 0.0 – 40.0 N/cm² with the pressure resolution of 1.0 N/cm^2. The output pressure-recording rate can be set at 5, 10, 25, 50, and 100 Hz. It is powered with rechargeable PD2032 coin cell with operating time 48 h (5 Hz), 29 h (10 Hz), 11 h 36 m (25 Hz), 5 h 48 m (50/100 Hz), depending on the pressure-recording rate.

The built-in 3D MEMS accelerometer has an acceleration output of ±2, ±4, ±8 g (7bit) per axis. The accelerometer is preprogramed to make insoles ready (by shaking) for the experiments. The pressure data can be stored on board or transferred wirelessly using ANT radio (2.4 GHz) within the range of 2-5 m. The vertical foot force is also calculated (and logged) by using area of individual pressure sensor and pressure observed by them. The durability of these insoles is around 100km of walking/ running and the accuracy in peak total force measurements in walking is ±25% [35].

It is also possible to analyse plantar pressure distribution, gait lines, and overall center of pressure but in this thesis project work only vertical foot force and pressure is useful in order to determine ground contact events, GCT and gait phases. These insoles are available in nine different sizes, but we have used EU - 42/43 size insoles for experiment purposes since both subjects have similar foot size. Correct foot insole size provides good fitting inside the shoe of similar size. The individual pressure sensor and accelerometer placement can be seen in Figure 7.

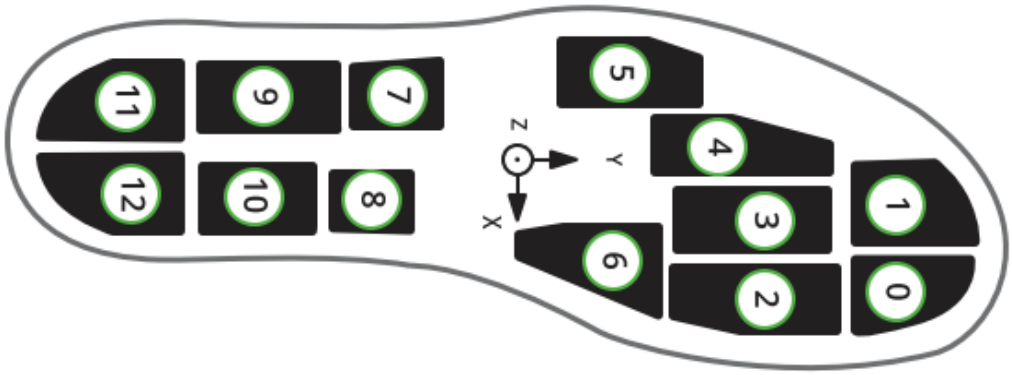

Figure 7. *Pressure sensor arrangement and foot accelerometer placement in Moticon insole, source [74]*

Each experiment was performed after placement of newly charged coin batteries inside the insoles. These Moticon insoles were fitted inside Asics-DS-trainer-16 neutral running shoes by replacing the original insoles. The foot pressure of each insole was zeroed after putting on the shoes but keeping the foot above the ground. After pressure zeroing, it was checked that the insoles were working well by applying some foot force on ground and looking at the force patterns in wirelessly connected cell phone. Both insoles were turned ON before starting the experiment. The data synchronization between both foot (also with INS/GPS data) was achieved by making synchronous (both feet at same time) vertical jumps in the beginning, during, and at the end of the experiment. The relative timing accuracy of the insoles data recording is 2/(pressure-recording-rate) therefore these synchronous jumps helped a lot to correct the timing errors.

3.4 Gait Segmentation Method

The gait segmentation is a way to divide the motion data parameters into repetitive cycles based on repetitive gait features (normally foot contact events). There are several human gait partitioning methods existing based on the both wearable and non-wearable sensors [58]. The use of inertial sensors (wearable) has become popular in the recent years. This thesis describes the details of a novel vertical velocity based algorithm for gait stride segmentation first reported in Davidson et al. [55]. This step segmentation uses the periodicity of vertical velocity, measured by back-mounted INS/GPS data logger.

The stride segmentation, an extension of the step segmentation algorithm, combines two consecutive segmented steps. Therefore, the segmented step has one repetitive pattern of the vertical velocity, as in Figure 5 and Figure 6 by Davidson et al. [55]. However, each segmented stride has two repetitive patterns of the vertical velocity. The pseudo code of algorithm to find step and stride indices is written in Table 4.

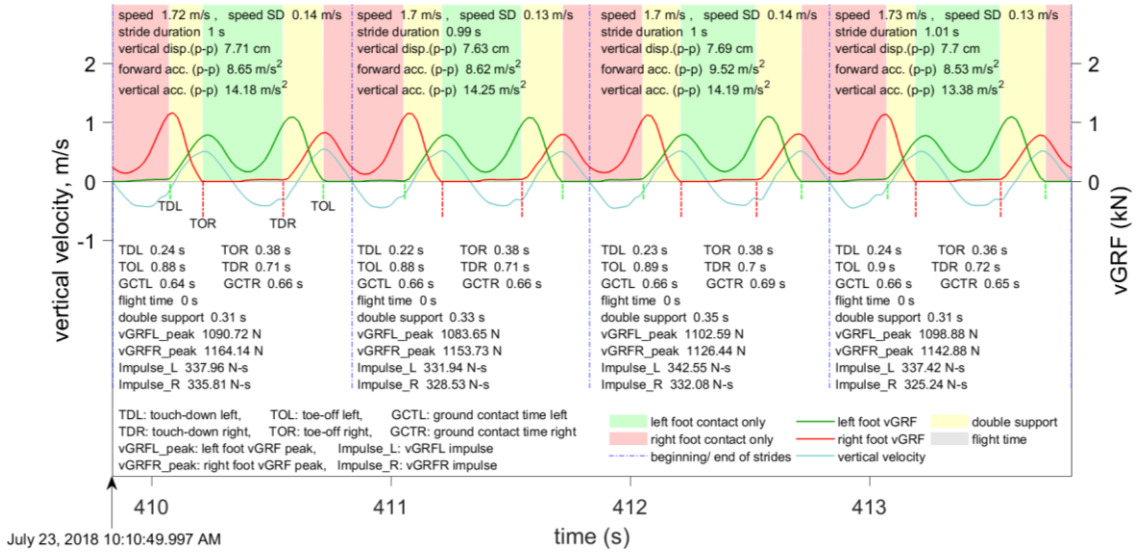

Figure 8. *The stride segmentation (blue dashed lines) by using vertical velocity during walking. The INS/GPS metrics of five parameters are displayed for each stride in upper section of plot. The lower section has twelve metrics parameters from Insoles*

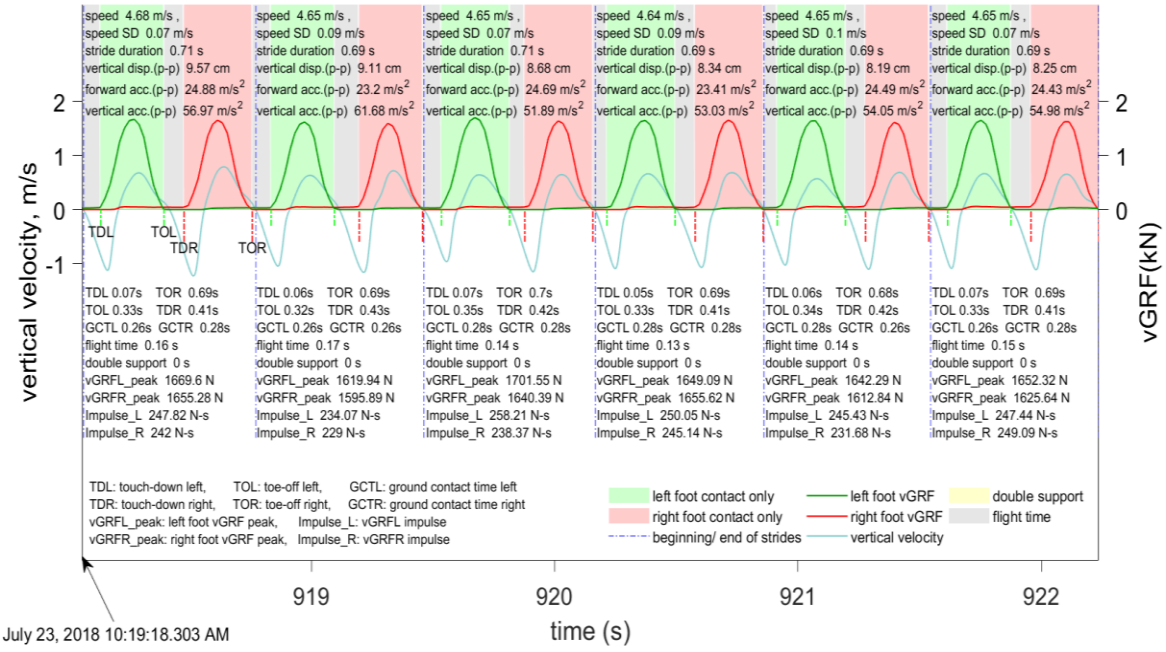

Figure 9. *The stride segmentation during running is also based on the vertical velocity. Curves and metrics as in Figure 8*

It can be seen in Figure 8 and 9 that each gait-stride comprises two complete cycles of vertical CoM movement. In addition, a complete left footstep is also present in each stride, during both walking and running. Each stride comprising a complete left footstep

is accomplished by the algorithm (Table 4) when combining two adjacent velocity segmented gait-steps we make sure that first step has a TDL so both steps combined can form a stride which has a complete left footstep. A velocity segmented footstep having initial TDL or TDR is determined by using ground-track-oscillations since ground-track-oscillations is positive near TDL and negative near TDR.

Table 4. Gait Segmentation Algorithm

Algorithm1	Vertical velocity-based gait segmentation algorithm (pseudocode)
1:	Initialize and assign variables*: SP, GSP, GT, VV, VD, SC, and I*
2:	**Comment**: Variables '*VV*' and '*VO*' are high pass filtered vertical velocity and peak to peak body CoM oscillation (vertical oscillation) vectors (1 × N) respectively. The return variables are, '*I*' is total count of events when vertical velocity is zero during walking/ running, '*SP*' vector contains indices of step segmentation points (when vertical velocity is zero with negative slope when body CoM is furthest from surface) and 'SC' is total number of steps counted. '*GSP*' vector contains indices of stride (alternate step) segmentation points and 'GT' is ground track oscillations.
3:	**procedure** velocityBasedStepSegmentation (*VV*, VD)
4:	***for*** *k = 1: N-1*
5:	***if*** $VV_k < 0$ *and* $VV_{k+1} > 0$ *and* $VD_k < 1.0$
6:	*I = I + 1;*
7:	***end if***
8:	***if*** $VV_k > 0$ *and* $VV_{k+1} < 0$ *and* $VD_k > 1.0$
9:	**comment**: velocity index when velocity is around zero, velocity slope is negative and vertical distance is more than +1 mm (person moving)
10:	*I = I + 1;*
11:	*SP = [SP k];*
13:	***end if***
14:	***end for loop***
	SP = SP(2:end-1); **comment**: ignore first and last segmented (possibly incomplete) step
15:	*SC = length(SP) - 1 ;*
	If *GT(SP(1)+50)>0*
	SP = SP(2:end); **comment**: skip the first step
	end if
21.	***If*** *GT(SP(1)+50)<0* **comment**: to make sure that the stride has one complete left foot step.
22.	***for*** *k = 1: ceil(length(SP)/2)* **comment**: combine two steps to form a stride
	*GSP(k) = SP(2*k-1);*
	end for loop
23.	***end if***
25.	***return*** *< SP , GSP >*
26.	**end procedure**

3.5 Gait Metrics

The slope of vGRF curves is used to detect the TD and TO events for both left and right foot. These events can be seen in Figure 8 and 9, along with foot contact by means of color shading. For example, light green (only left foot is in contact with ground), light red (only right foot is in contact with ground), light yellow (double support, both feet are in contact with ground), and light gray (flight time, both feet are in air). Several gait timings

and foot force parameters (temporal features) can be derived by using the details of vGRF strides segmented from vertical velocity-based method, such as: TD time, TO time, GCT, peak vGRF, impulse for both feet, along with flight time and double support time. Other important metrics components which can be calculated after the gait segmentation are mentioned below:

Stride duration: The time duration from beginning of the stride to beginning of the next stride.
Cadence: Rate of strides covered per minutes (1/stride duration).
Stride length: The forward distance covered during the complete gait stride.
Speed difference: The difference of maximum and minimum speed during stride.
Vertical displacement: The peak to peak displacement of CoM during a stride.
vGRF features: TO and TD events with respect to beginning of the gait strides. In addition, GCT, flight and double support time of each stride.

3.6 Dataset Description

The repetition of foot strides is what makes a gait cycle. In general, the gait cycle can be classified into walking, speed-walking, jogging and running according to gait speed. However, there is not a fixed criterion for speed-based classification. An alternate way to identify the walking and running mode is by type of foot landing (TD).

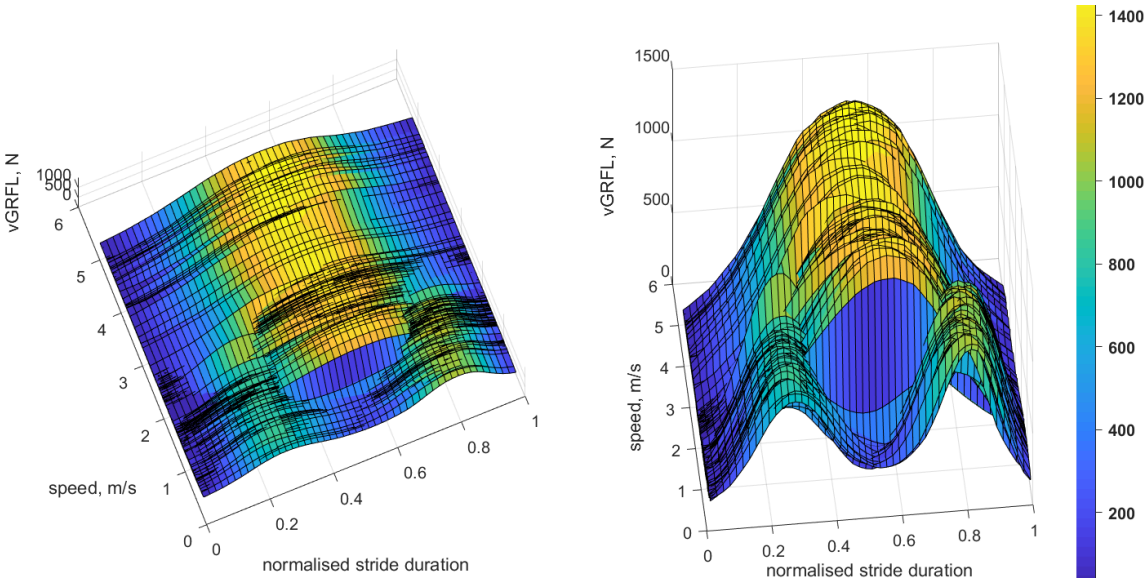

Figure 10. *Left-foot strides with normalised stride duration from test dataset-2*

In running, higher impulse (than walking) is required to achieve greater speed, even with shorter stance time (than walking). Therefore, only a single vGRF peak is formed in vGRF stride curves in running, compared to two vGRF peaks in walking. Rear foot landing results in two peaks (braking and propulsive force peaks) in vGRF curves and during

fore/mid- foot ground landing only one vGRF peak is observed. The rear foot landing is characteristic of slow and speed-walking, whereas fore foot landing is common in jogging and running. The type of foot landing can be determined for running (heel strike, forefoot-, midfoot-touch-down). The classification in Figure 10 (two different curves) is based on only two classes: walking and running, where segmented strides are plotted to compare the average forward speed and vGRFL by means of normalized stride duration.

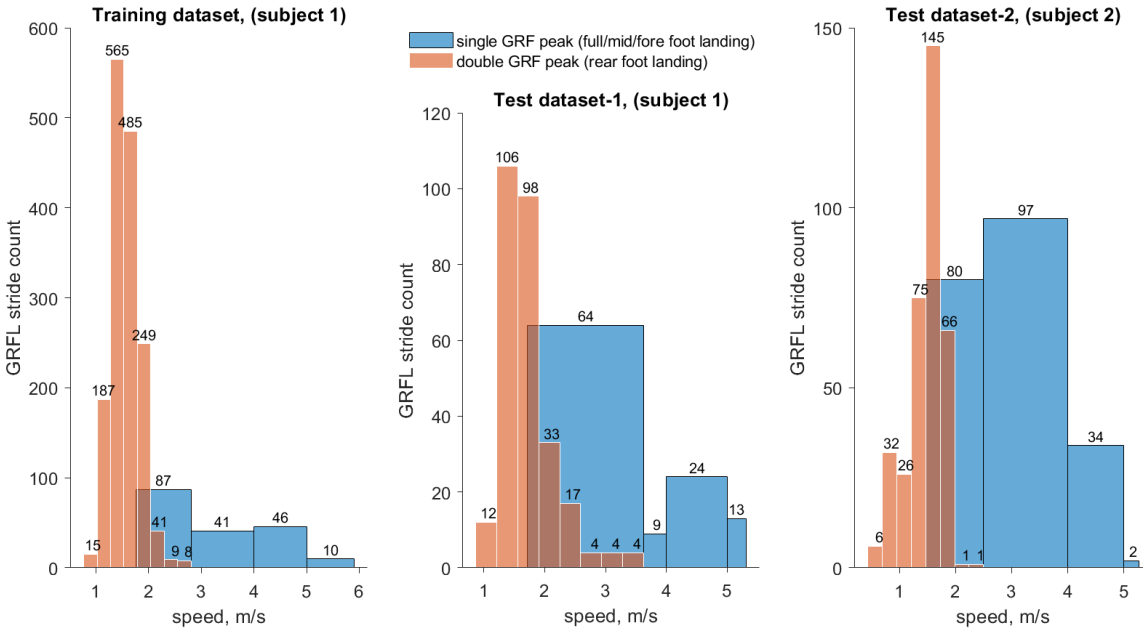

Figure 11. *Dataset description (speed vs foot-landing type)*

Research experiments reported in this thesis includes two healthy adult participants (subject-1, male–72kg–178cm and subject-2, male–64kg-170cm) for the motion data collection. The style of data logger mounting, shoes and running track were kept unchanged during the data acquisition for both test subjects. The INS/GPS logged data was manually synchronized with moticon's vGRF data and after the gait segmentation, three different datasets were prepared. The 'training dataset', used for machine learning based algorithm, consists of 1743 gait strides of walk-run by subject-1, whereas, 'test dataset-1' and 'test dataset-2' are set of 388 strides of subject-1 data and 565 strides of subject-2 data respectively. The stride collection of each stride dataset is extracted from continuous motion data of single walk-run with varying speed and contains strides during walking, speed-walking, jogging and running. Further details of the average speed distribution of each dataset is displayed in Figure 11, along with the type of foot landing by means of peaks in vGRF. It can be seen that speed-walking and jogging have overlapping speed.

4. INDIRECT ESTIMATION OF GCT, VERTICAL GRF

The temporal/ spatiotemporal parameters can be calculated by using the insoles data. It is common knowledge that the foot movement has correlation with INS/GPS device (CoM) movement since the body motion is analogous to damped spring motion. Therefore, our approach is to develop a machine learning model to predict foot parameters and complete vGRF curve by using INS/GPS data. The vGRF curves (vGRFL and vGRFR) are continuous during locomotion and the shape of the vGRF curves changes with walking style and speed. The continuous variability in the human motion makes it a complex task to predict the continuous point to point vGRF magnitude by using corresponding kinematic features from INS/GPS data logger. Therefore, one possible approach can be to predict vGRF stride curves for each segmented gait stride (best match from pool of training set) and combine all predicted (best matched) gait stride curves to reproduce the continuous vGRF plot. This approach has been elaborated in section 4.1. Alternate approach is time series prediction by means of deep neural networks which makes it possible to predict each point of vGRF curves based on the current and immediate past of INS/GPS logged data parameters; this is elaborated in section 4.2.

4.1 Machine Learning Implementation

The velocity-segmented gait strides, as in Figure 8 and 9, consist of two repetitive patterns in parameters acquired from INS/GPS and one repetitive pattern in vGRFs. This repetitiveness in both left and right foot vGRF strides is the reason why stride segmentation is preferred over step-segmentation for machine learning implementation. The repetitiveness of vGRFL and vGRFR helps machine learning methods to identify the closest match based on their features. Figures 8 and 9 display stride segmentation plots for walking (four strides) and running (six strides) using the same data that was used for step segmentation in Figure 5 and 6 in Davidson et al. [55]. Moreover, there is synchronization of acquired data from INS/GPS with instrumented insole's data (vGRF); therefore, the segmentation of vertical velocity strides also creates the corresponding stride vectors for each INS/GPS data vector along with vGRF stride vectors (vGRFL stride and vGRFR stride) as described in section 3.1 and section 3.6. These vGRF strides have correlation with the corresponding segmented data vectors logged from INS/GPS data

logger. Although it is possible to further process and derive numerous body kinesiology feature vectors by using acquired INS/GPS data including vital ones detailed in Section 3, additional features can be derived by calculating average, standard deviation, peak to peak (p-p) magnitude of segmented stride feature vectors.

4.1.1 Input feature extraction and optimal selection

The data processing results (Figure 13) show that several features of segmented INS/GPS data have been found that correlate with respective Moticon's vGRF stride features (foot parameters). Therefore, it is possible to predict the target vGRF features along with vGRF curves by using the INS/GPS acquired data. The target output feature list includes parameters which can only be extracted from insoles i.e. touch-down time, toe-off time, ground contact time, peak vGRF, impulse, flight time and double support time. Furthermore, in machine learning, optimal feature selection is important in order to make simple and reliable prediction models. Strong positive and negative correlation between input and target features is equally important. Moreover, the optimal input features are selected in such way that they are not derived from each other (this is the reason they are called optimal), i.e. input features with high correlation among them can decrease the accuracy of trained model with unseen (test) data.

It has been shown in literature [44] and is a well-established fact that the speed is negatively correlated with GCT and double support time; speed is however positively correlated with flight time, peak vGRF, and impulse. In order to have a big picture of correlation among all the input features, the absolute correlation among input features has been shown as a colormap in Figure 12. Each cell in the colormap represents the absolute correlation between the features intersecting at that cell. The minimum to maximum absolute correlation range (0 to 1) has been shown with the help of 10 different colors.

A few observations regarding Figure 12 and rules considered for optimal feature selection are following:

- The features derived from 3D-angles and 3D-angular velocity are not considered because, first, angle oscillations are dependent on the orientation of the VN-200 and second, angular velocity vectors are logged in sensor frame (and not transformed into anatomical frame) making these also dependent on orientation. Therefore, even if the device is tightly mounted on the back there is a chance of disorientation. Also, the data of subject-2 is acquired with different sensor orientation than data of subject-1.

- The input features derived by using standard deviation (of stride data vectors) are highly correlated (>0.9) with corresponding range (p-p) input features. Therefore, if two input features have higher absolute correlation (>0.9) then it is wise to drop one of those.

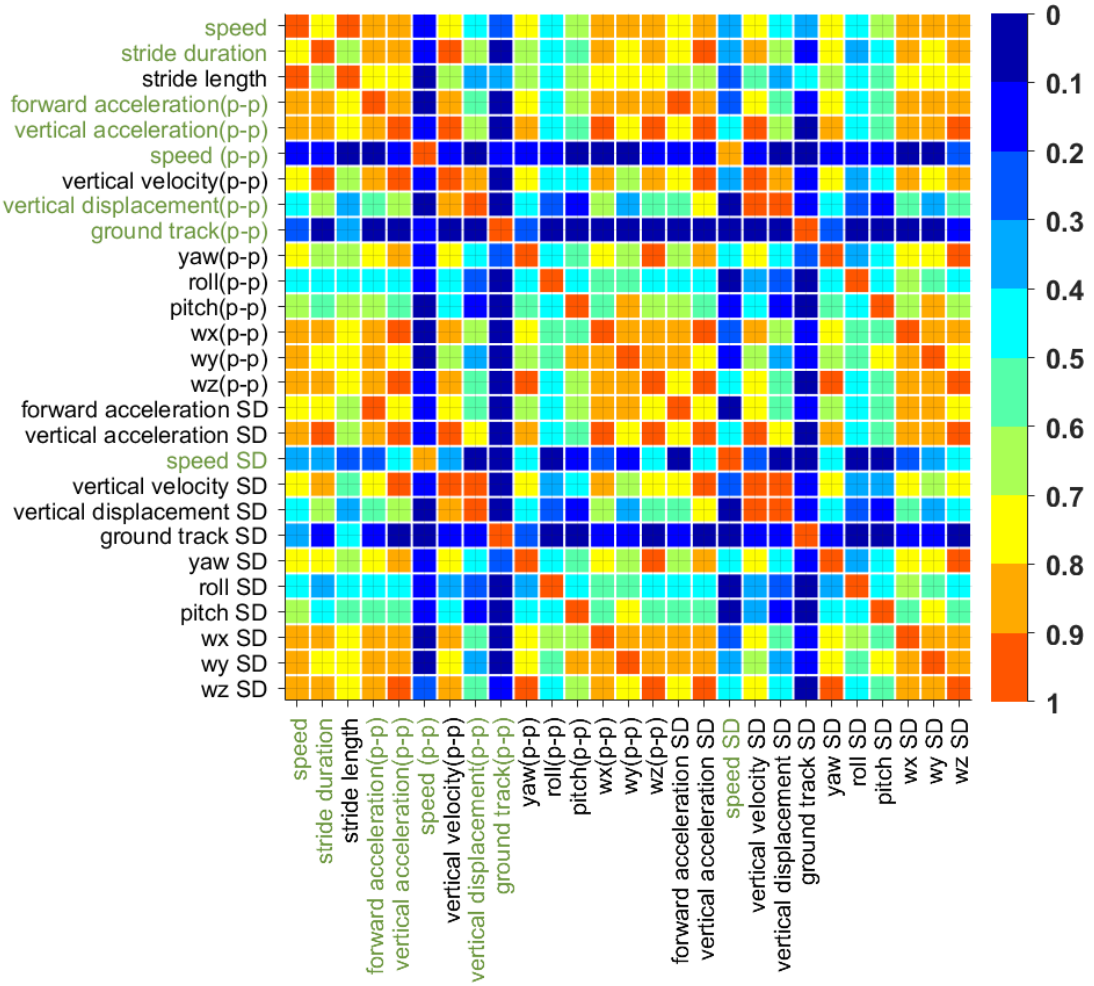

Figure 12. *Absolute correlation among all input features to identify optimal features*

After the first stage of input feature selection, the optimum feature set comprises speed, stride duration, forward acceleration (p-p), vertical acceleration (p-p), speed (p-p), vertical displacement (p-p), ground track (p-p) and standard deviation of speed vector. The correlation between selected optimal input and output features is shown in Figure 13.

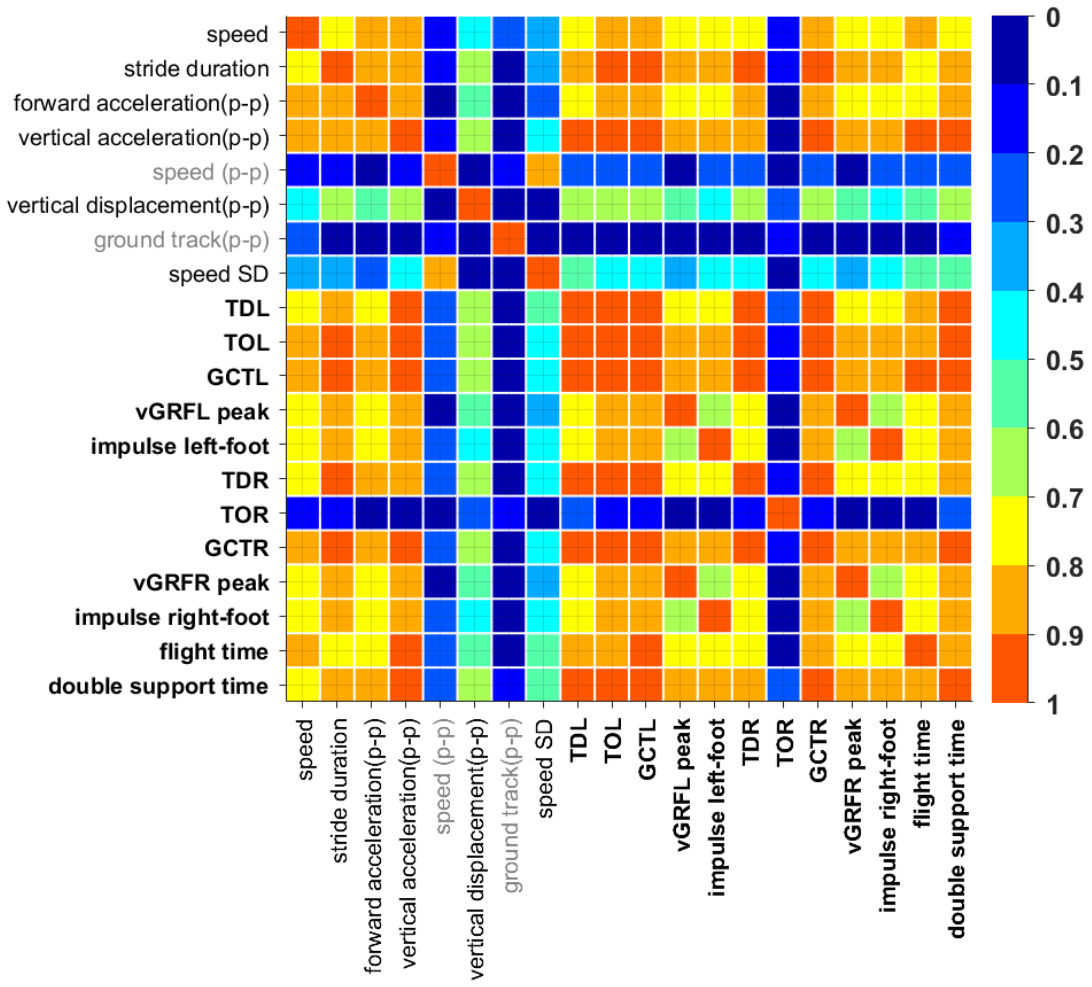

Figure 13. *Absolute correlation between optimal input and* ***target features***

- It can be seen in Figure 13 that speed (p-p) and ground track (p-p) do not have higher absolute correlation with other input features but they also do not have sufficient correlation (>0.5) with target parameters. So, these two parameters, having less correlation than 0.5 with each target output parameters, are also omitted from optimal input feature list.

The optimal feature list has only six features after removal of the two mentioned above. Therefore, the reduced optimal feature list includes speed, stride duration, forward acceleration (p-p), vertical acceleration (p-p), vertical displacement (p-p), and standard deviation of speed. Further observation of Figure 13 makes it clear that the toe-off time of right foot (TOR) does not show good correlation with input features and prediction results of TOR confirms that this feature cannot be predicted with accuracy. Therefore, TOR is omitted and finally 11 target features are retained.

4.1.2 Prediction of temporal features using multivariate linear regression (bagged ensembles)

MATLAB's regression learner app has been used to train 11 different regression models for target foot gait parameters namely TDL, TOL, GCTL, peak vGRFL, impulse of left-foot and same parameters for right foot except TOR. Flight time and double support time can also be predicted with sufficient accuracy, even though they are dependent on movement of both feet. The regression models of peak vGRFs and impulse (for both feet) are trained after normalization of target parameters (normalizing by BW) in order to make these prediction models independent of person's weight. In order to verify the method of feature selection, three types of regression models are trained for all 11 target parameters:

- Ensemble bagged trees (min. leaf size: 8 with 30 learners) by considering 6 optimal features as input.
- Ensemble bagged trees (min. leaf size: 8 with 30 learners) by considering PCA with 6 numeric components.
- Ensemble bagged trees (min. leaf size: 8 with 30 learners) by considering all 27 features as input.

4.1.3 vGRF feature prediction results

The prediction results of foot parameters by means of INS/GPS and bagged ensembles for both subjects are presented in this section. The training data is from subject-1 but trained models are applied to test data from both subject-1 and subject-2. Both subjects have different BW and height therefore they might have different gait characteristics as well. This is confirmed from Figure 14 and Figure 15 since all 11 foot parameters have better accuracy with test data from subject-1. As we have already discussed that some parameters, having BW dependence, are trained after normalizing by BW such as the peak vGRFs (vGRFL_peak and vGRFR_peak) and foot impulses (impulse_L and impulse_R). By training the models for normalized target parameters helps to estimate those target parameters of another subject with different BW. After making normalized target parameter prediction for different subject, the actual target parameter estimation is obtained by multiplying the BW of that subject.

Furthermore, after studying both training and test errors (shown by dark and light colors, respectively in Figure 14 and 15) for three different types of feature selections namely; 6

optimal features (green), 6 component features from PCA (red) and all 27 features (blue). For majority of target parameter predictions, the normalized-root-mean-square-error (NRMSE) is minimum when the model is trained with optimal features as input features.

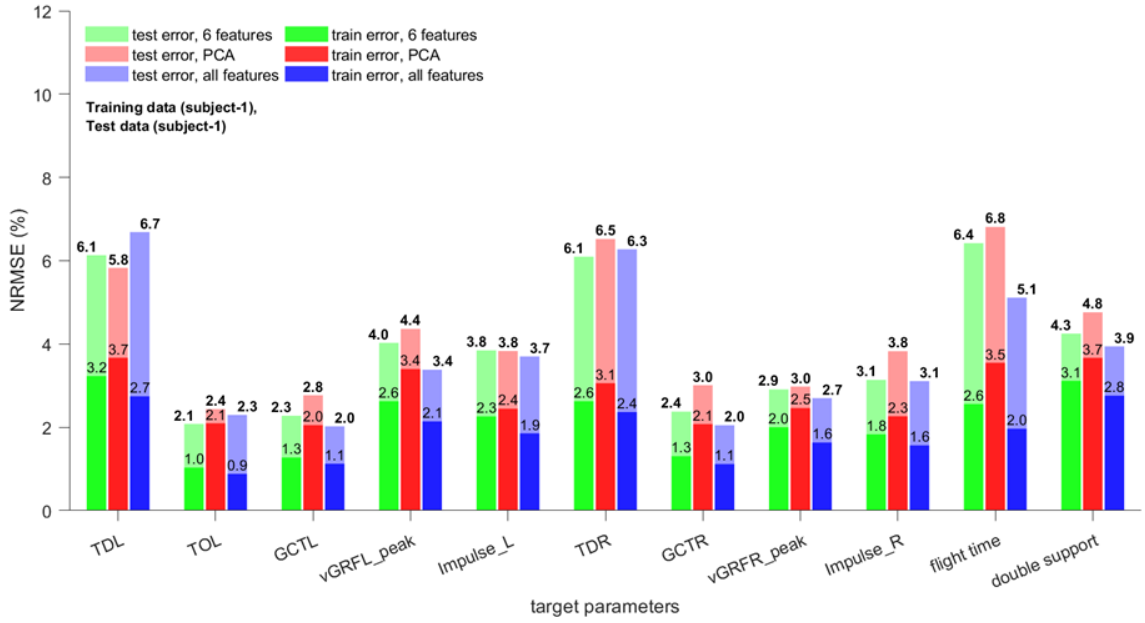

Figure 14. *Performance of trained regression models with train dataset and test dataset-1 for foot feature predictions*

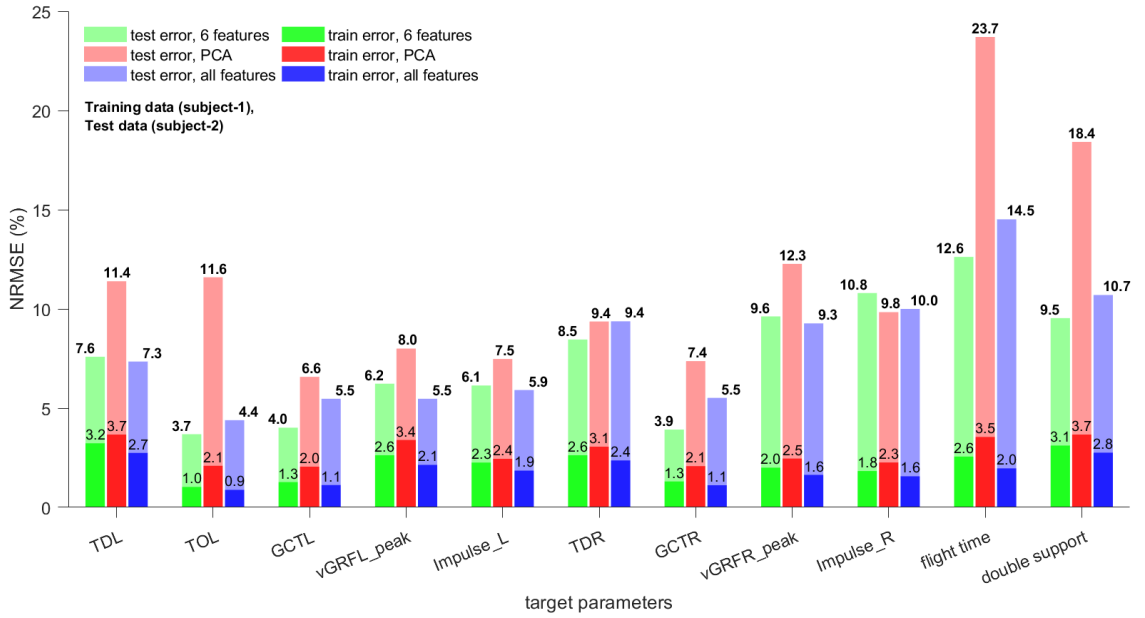

Figure 15. Performance of trained regression models with train dataset and test dataset-2 for foot feature predictions

It is also very important to notice that the TD and TO parameters are dependent on the stride segmentation method since they are events and their time is measured with respect to the beginning of the gait strides. On other side, the GCT, peak vGRF and foot impulse depend on the complete stride vector and should have less variability on the stride segmentation method. The NRMSE for GCTL and GCTR are found to be, 2.3% and 2.4% for test dataset-1 (subject-1) and, 4.0% and 3.9% for test dataset-2 (subject-2). Furthermore, The NRMSE for vGRFL_peak and vGRFR_peak is found to be, 4.0% and 2.9% for test dataset-1 and, 6.2% and 9.6% for test dataset-2. Finally, The NRMSE for impulse_L and impulse_R are found to be, 3.8% and 3.1% for test dataset-1 and, 6.1% and 10.8% for test dataset-2.

4.1.4 vGRF curve prediction approach (kNN) and results

The vGRF strides have two distinct characteristics, height (peak vGRF) and width (stride duration, GCT, TO and TD). In order to construct vGRF curve, the selection of each vGRF stride has to be done precisely in order to match both peak vGRF and timing parameters. Our approach is to find a vGRF stride match with closest possible time parameter matching (not considering peak vGRF since it has different scale).

The k nearest neighbor approach has been used to pick a target vGRF stride from a pool of training strides. The BW normalized vGRFL and vGRFR training strides are divided into separate collections and their respective foot timing parameters (TO, TD, GCT and stride duration) are used as input parameters to calculate euclidean distance. For left foot vGRFL strides, the input feature space includes stride duration, TOL (predicted as in section 4.1.3) and GCTL (also predicted). The parameter TDL is omitted because of large inaccuracy in its prediction. Similarly, for right foot vGRFR strides, GCTR (predicted) and stride duration are considered as input feature space. For every test data stride, the timing parameters are calculated (stride duration) or estimated (TO, TD and GCT) with regression ensemble methods. The stride index of the k best match vGRFL and vGRFR stride curves are sought and are averaged to get closest prediction of vGRF strides. The optimum k number of neighbors found are 5 to 12. The NRMSE for test dataset-1 (subject-1) for continuous curve generation are vGRFL: 6.63% and vGRFR: 5.37% with eight (k=8) neighbors.

4.2 Deep Learning Implementation

One approach of the predicting each stride, namely machine learning, has been discussed in the section 4.1, but it is highly dependent on the size of training dataset and it does not generate new strides therefore it is impossible to detect new patterns in force curves. An alternative approach is time series analysis by means of neural network to predict point to point vGRF curves based on the current and immediate past of INS/GPS logged data parameters. The GCT can also be estimated, by using deep learning method, by considering GCT label 1 when the foot is in contact with the ground and 0 when foot is off the ground. The GCT-labels are derived by post processing of the moticon's vGRF and foot pressure data. The raw measurements of INS/GPS parameters are used as input data to predict the continuous vGRF and GCT (label) curves acquired by the Moticon insole.

The training data for neural network models is kept same as the machine learning approach mentioned in the section 4.1 to facilitate comparison of the results obtained from the two methods. That means, the unsegmented/ continuous data acquired from subject-1 has been used for the training. The training data has 725,017 consecutive samples with the date rate of 400Hz. It is interesting to notice that 1743 gait strides are extracted from this continuous dataset which results in average stride duration of 1.039 seconds.

The neural networks can be trained better and made responsive to even slight changes if the input data has required variety in it. The training data which we have used contains the speed from 0.77 to 5.90 m/s. One approach for vGRF and GCT estimation for our setup by neural networks has already been discussed in [55]. As it is a time series problem to predict continuous vGRFs and GCTs, the recurrent neural network is a potential solution. But, long term dependence of the current vGRF and GCT on the past data points suggests that the LSTM or GRU [55] may lead to better predictions than vanilla RNN. In this section, a LSTM implementation is presented.

We have trained two separate LSTM neural network regression models for vGRF and GCT predictions. The training software we have used is 'keras' [75] with Google's TensorFlow running in background. The training data consists of 6 input data vectors and 2 target output data vectors. The target output feature vectors are vGRFL and vGRFR in case of vGRF curve predictions and GCTL-label and GCTR-label in case of GCT label predictions. The input features are 3D acceleration and 3D angular rates. The feature selection is done based on the 'consider only one' and 'leave one out' approach. It was found that the forward and vertical acceleration are most important input vectors, in terms

of high dependence, to predict the vGRF and GCT labels. The addition of lateral acceleration and 3D angular velocity also improves the prediction to some extent. Further input features, in addition to 3D acceleration and 3D angular rates, don't improve the prediction accuracy significantly.

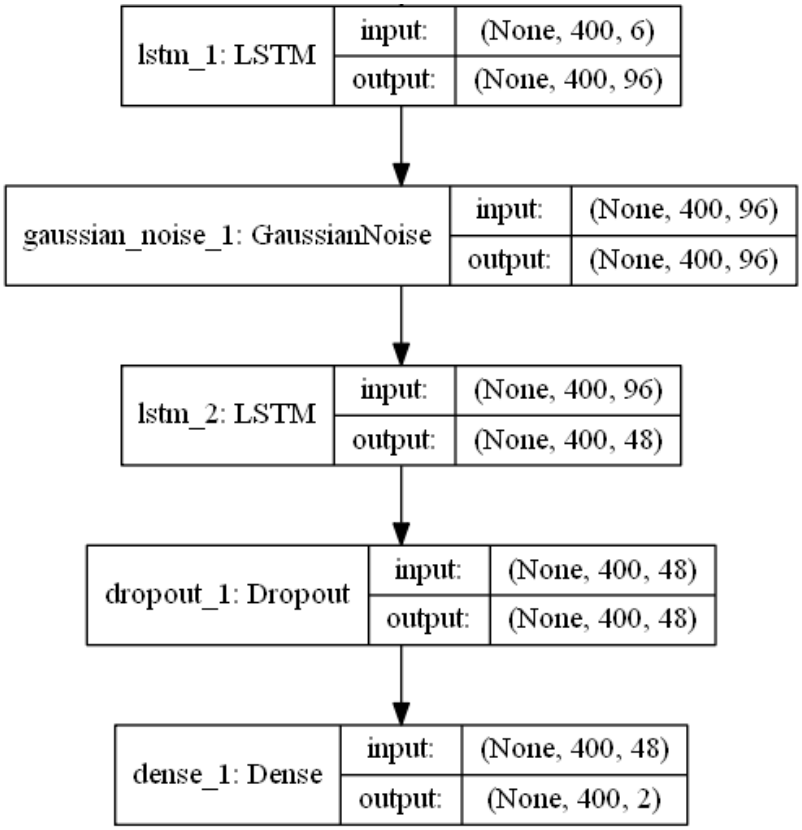

Figure 16. Neural network model diagram based on LSTM

There are many possibilities to explore when constructing the neural network models. Several combinations of LSTM and GRU layers were tried by considering the different number of neurons in layers and by changing the hyperparameters. It was found that if a model has enough neurons to learn sufficient features of input data then there is a possibility to generate several neural network models with small change in structure (by means of number of neurons) and they may provide similar prediction results given that proper training is performed for each variant. The used neural network model structure is shown in Figure 16.

The considered neural network configuration has two LSTM layers along with one input noise layer (to improve robustness towards test data noise), one dropout layer (to drop the neurons during training epoch) to improve generalization and a fully connected dense layer to map the hidden layer data to the two independent target outputs. The noise layer, which applies additive zero centered gaussian noise, is a way to intentionally corrupt the

input data to mitigate the model overfitting and is also known as noise regularization. If the gaussian noise layer is applied before an RNN layer, then it is called RNN noise regularization. It is only activated during the model training. Moreover, the dropout layers randomly select the neurons (based on dropout rate) to ignore them during the training. In this dropout regularization, dropped neurons have no effect on the activation of neurons in downstream layers during that training epoch. The dropout layer is also activated during the model training only.

The input data vectors, (all measured 3D accelerations and 3D velocity, 400Hz) are first scaled between -1 to 1 and then are divided into sequences of 400 samples with shift of one data point for each new sample. In other words, there is an overlapping of 399 sample point between two consecutive sequences. The decision of having 400 sample points in sequence was taken by considering the average strides duration of the training data which is 1.039 seconds i.e. there are 400 samples in each stride approximately. The sample size of 400 results in having 724616 training sequences of input data sequence size of 400x6 and target data sequence of 400x2. In each sequence, the first 399x6 sequence points are history data (allowing the network to see in past to make current prediction) and 400^{th} is present input therefore when calculating the loss function the initial 399x2 points of estimated sequences are ignored keeping only the present prediction output points. In addition, by having 400 points in a sequence, it is not possible to make predictions for initial 399 example points in the train/test dataset.

The vGRF neural network model structure is similar to the GCT-label prediction model with the difference of activation function. The fully connected dense layer in vGRF model has rectified linear unit (ReLU) activation function whereas in the GCT-label model the sigmoid activation function is used. In addition, both models use ‘adam’ optimizer with ‘mean_squared_error’ loss function for the vGRF and ‘binary_crossentropy’ for GCT-label. When models are trained, the continuous point to point vGRF and GCT-labels can be predicted without any direct measurements of foot pressure from insoles.

The GCT-label prediction is a binary classification problem therefore sigmoid activation function (at output layer) is preferred over softmax. The use of softmax activation function requires 2 output neurons for each target variable and output prediction of labels is also noisy (wrong label prediction) near TD and TO. In contrast, the sigmoid requires a single output neuron for each target label and has the range (0,1).

The GCT-label prediction probabilities of test dataset-1 for binary classes label-1 and label-0 are displayed in Figure 17. The RMSE for left and right foot GCT-label predictions

are 0.26 and 0.28, respectively. The binary foot contact labels can be obtained by creating a probability threshold at 0.5 for binary decision. The final output binary labels after applying threshold of 0.5 is shown in Figure 18. The accuracy for left and right foot binary GCT-label predictions are 92.65 and 91.23, respectively. Most prediction errors are during the TO and TD events, when foot transition is ongoing.

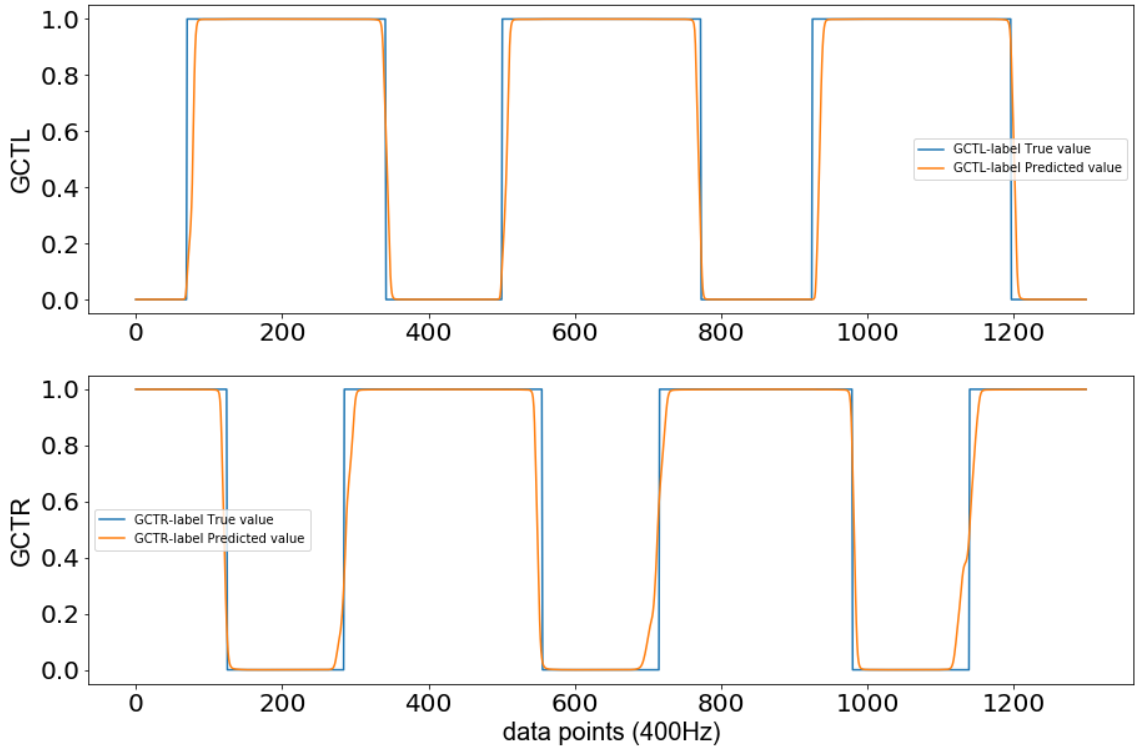

Figure 17. *GCT-label prediction (binary classification probability) glimpse for test dataset-1.*

The vGRFL and vGRFR prediction curves for test dataset-1 are plotted in Figure 19. It can be seen that the estimated vGRF curves accurately approximates the true vGRF measurements. The NRMSE in vGRF prediction for test dataset-1 is 8.38% and 8.54%, respectively.

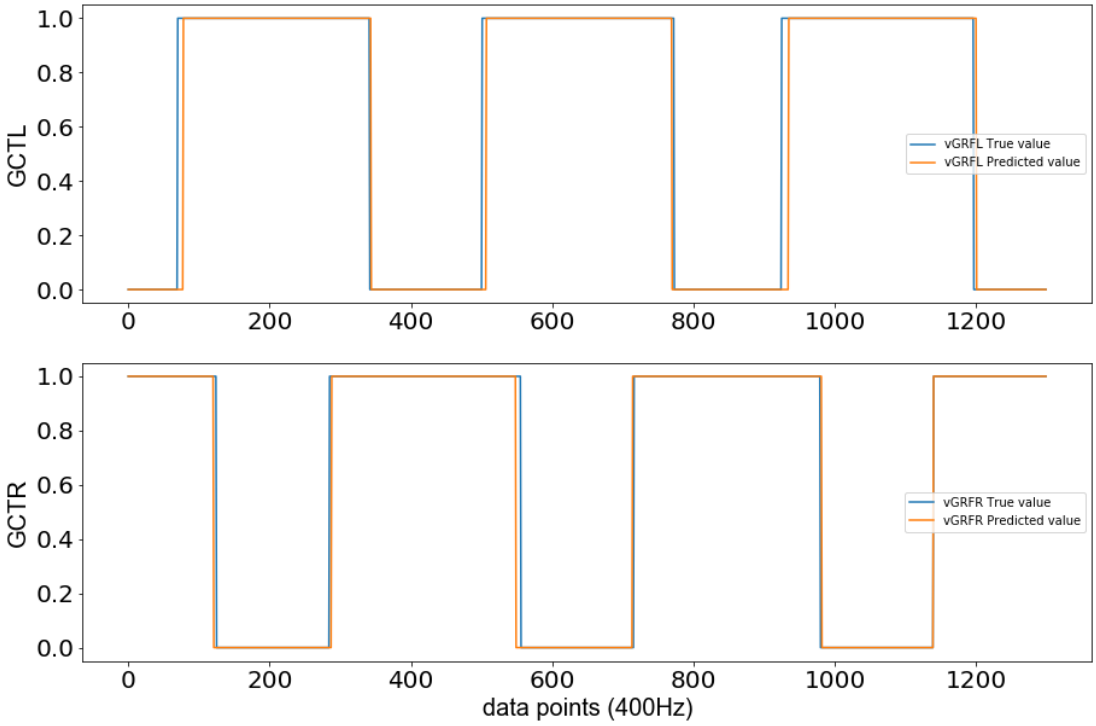

Figure 18. *GCT-label prediction (binary label classification by applying threshold at 0.5) for test dataset-1, same data as in Figure 17.*

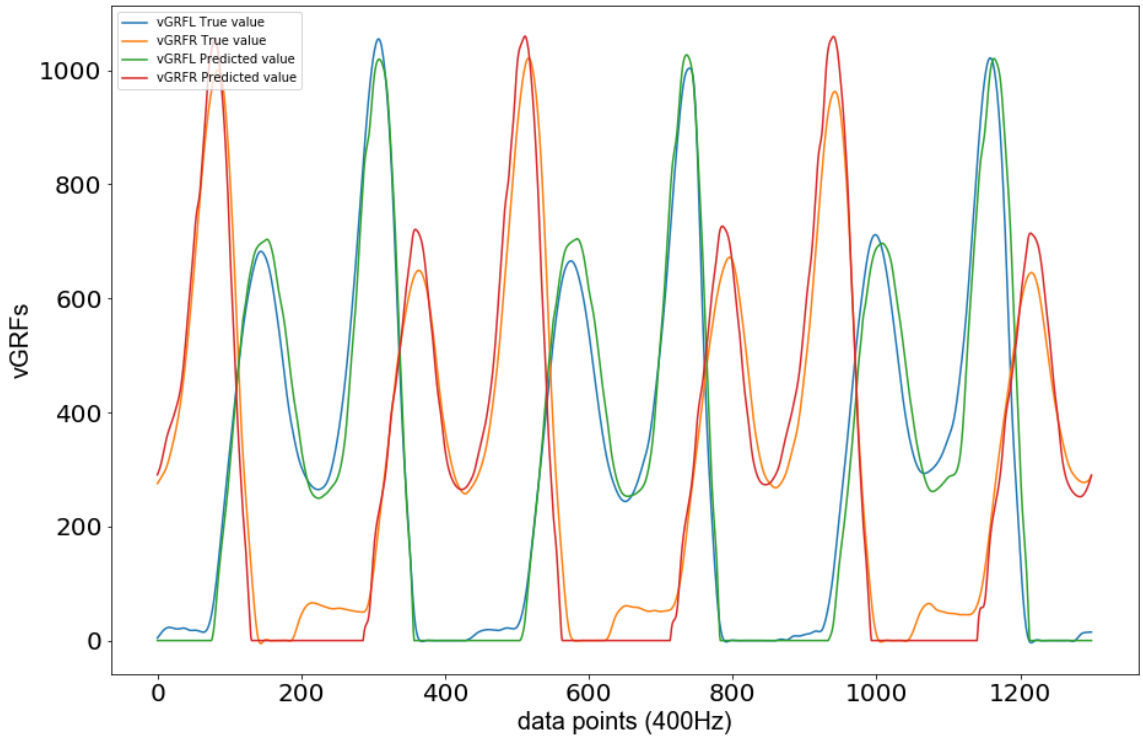

Figure 19. *vGRF predictions by the LSTM neural network for test dataset-1.*

5. CONCLUSIONS

This thesis presents methods for the human gait metrics components calculation and estimation by means of motion data capture using high precision single body mounted accelerometers, gyroscopes and GPS receiver. The use of advanced INS/GPS sensor benefits us through high accuracy in measurements of acceleration and angular velocity which is key for intra-stride gait details. Further, a detailed description of novel gait stride segmentation has been presented which does not require any foot pressure information to perform the gait segmentation. The gait segmentation of logged data vectors makes it possible to calculate majority of gait metrics parameters except GCT and vGRF. The gait metrics are essential to examine the runner's performance and can be used for bio-mechanics research. The remaining metrics components, i.e. GCT and vGRF, can be estimated by applying the techniques of both machine learning and deep learning. The unique patterns in logged data have been identified and based on these features, a bagged regression tree method is used for indirect estimation of GCTs and vGRFs. It has also been demonstrated that some features among TO, TD, impulse, flight time and double support time can also be predicted with good accuracy even for different human subject with known BW. Moreover, an approach to construct vGRF curve by using the kNN is reported.

Another approach for point to point vGRF and GCT label prediction is also shown by using the deep learning. An LSTM type model is presented for prediction of both continuous vGRF and GCT-labels. The two indirect estimation methods are proofs of concept that accurate prediction of foot features is possible without using the foot pressure sensor. The results are reproducible if the accuracy of logged data remains the same.

6. FUTURE WORK

There are some approaches which can be used to improve motion data logging and foot feature estimation techniques that were presented in this thesis. The DGNSS and RTK system can be used for better GPS accuracy which may result in more precise GPS acquired parameters. The verification of vertical distance and vertical oscillation measurements can be done by using state-of-the-art optical measurement systems. In addition, the moticon insoles are not the most accurate way to acquire the vertical foot pressure and vGRF data. There is a possibility of improving the accuracy of the training data by either using better insoles or calibrating the moticon insoles with force plates and making corrections to the moticon acquired readings. The robustness and generalization of prediction models can be improved by acquiring more training data and data from multiple subjects.

Further, there are possibilities to study and correlate the total energy consumption with running style. An extra accelerometer is present in the foot insole which hasn't been used and the data acquired from that accelerometer can be used for foot angle determination during the foot strike. Further possibilities are the miniaturization of hardware and real time logging of gait metrics for researcher and coaches. Finally, there is chance to improve the accuracy of estimation results presented in this thesis, by further in depth analysis and by using better estimation methods.

7. REFERENCES

[1] J. Nutt, C. Marsden, and P. Thompson, “Human walking and higher-level gait disorders, particularly in the elderly,” *Nuerology*, vol. 43, no. 2, pp. 268–279, Feb. 1993.

[2] “Strideway System,” *Tekscan*. [Online]. Available: https://www.tekscan.com/products-solutions/systems/strideway-system. [Accessed: 06-Apr-2019].

[3] K. Brütsch *et al.*, “Influence of virtual reality soccer game on walking performance in robotic assisted gait training for children,” *J. Neuroengineering Rehabil.*, vol. 7, p. 15, Apr. 2010.

[4] “Fitbit Help.” [Online]. Available: https://help.fitbit.com/. [Accessed: 04-Apr-2019].

[5] I. Bouchrika, “A Survey of Using Biometrics for Smart Visual Surveillance: Gait Recognition,” in *Surveillance in Action: Technologies for Civilian, Military and Cyber Surveillance*, P. Karampelas and T. Bourlai, Eds. Cham: Springer International Publishing, 2018, pp. 3–23.

[6] E. Ackerman, “DURUS Brings Human-Like Gait (and Fancy Shoes) to Hyper-Efficient Robots,” *IEEE Spectrum: Technology, Engineering, and Science News*, 12-Jul-2016. [Online]. Available: https://spectrum.ieee.org/automaton/robotics/humanoids/durus-brings-humanlike-gait-and-fancy-shoes-to-hyperefficient-robots. [Accessed: 04-Apr-2019].

[7] E. Ackerman, “IHMC Teaches Atlas to Walk Like a Human,” *IEEE Spectrum: Technology, Engineering, and Science News*, 05-Dec-2018. [Online]. Available: https://spectrum.ieee.org/automaton/robotics/humanoids/ihmc-teaches-atlas-to-walk-like-a-human. [Accessed: 04-Apr-2019].

[8] P. Fleming, C. Young, S. Dixon, and M. Carré, “Athlete and coach perceptions of technology needs for evaluating running performance,” *Sports Eng.*, vol. 13, no. 1, pp. 1–18, Oct. 2010.

[9] J. Wang, M. She, S. Nahavandi, and A. Kouzani, “A Review of Vision-Based Gait Recognition Methods for Human Identification,” in *2010 International Conference on Digital Image Computing: Techniques and Applications*, 2010, pp. 320–327.

[10] T. K. M. Lee, M. Belkhatir, and S. Sanei, “A comprehensive review of past and present vision-based techniques for gait recognition,” *Multimed. Tools Appl.*, vol. 72, no. 3, pp. 2833–2869, Oct. 2014.

[11] C. Prakash, K. Gupta, A. Mittal, R. Kumar, and V. Laxmi, “Passive Marker Based Optical System for Gait Kinematics for Lower Extremity,” *Procedia Comput. Sci.*, vol. 45, pp. 176–185, Jan. 2015.

[12] VICON, “Injury Prevention at the U.Calgary RIC,” *VICON*. [Online]. Available: http://www.vicon.com/case-studies/life-sciences/injury-prevention-at-the-ucalgary-ric. [Accessed: 06-Apr-2019].

[13] VICON, “Vicon Vero | Power. Flexibility. Motion Capture,” *VICON*. [Online]. Available: http://www.vicon.com/products/camera-systems/vero. [Accessed: 08-Apr-2019].

[14] VICON, “Motion Capture for Life Science,” *VICON*. [Online]. Available: http://www.vicon.com/motion-capture/life-sciences. [Accessed: 06-Apr-2019].

[15] P. A. Federolf, “A Novel Approach to Solve the ‘Missing Marker Problem’ in Marker-Based Motion Analysis That Exploits the Segment Coordination Patterns in Multi-Limb Motion Data,” *PLoS ONE*, vol. 8, no. 10, Oct. 2013.

[16] K. Aminian and B. Najafi, “Capturing human motion using body-fixed sensors: outdoor measurement and clinical applications,” *Comput. Animat. Virtual Worlds*, vol. 15, no. 2, pp. 79–94, 2004.

[17] L. C. Benson, C. A. Clermont, S. T. Osis, D. Kobsar, and R. Ferber, “Classifying running speed conditions using a single wearable sensor: Optimal segmentation and feature extraction methods,” *J. Biomech.*, vol. 71, pp. 94–99, Apr. 2018.
[18] C. Mitschke, T. Heß, and T. L. Milani, “Which Method Detects Foot Strike in Rearfoot and Forefoot Runners Accurately when Using an Inertial Measurement Unit?,” *Appl. Sci.*, vol. 7, no. 9, p. 959, Sep. 2017.
[19] J. Reenalda, E. Maartens, L. Homan, and J. H. J. Buurke, “Continuous three dimensional analysis of running mechanics during a marathon by means of inertial magnetic measurement units to objectify changes in running mechanics,” *J. Biomech.*, vol. 49, no. 14, pp. 3362–3367, 03 2016.
[20] W. Zijlstra, “Assessment of spatio-temporal parameters during unconstrained walking,” *Eur. J. Appl. Physiol.*, vol. 92, no. 1–2, pp. 39–44, Jun. 2004.
[21] A. M. Sabatini, C. Martelloni, S. Scapellato, and F. Cavallo, “Assessment of walking features from foot inertial sensing,” *IEEE Trans. Biomed. Eng.*, vol. 52, no. 3, pp. 486–494, Mar. 2005.
[22] M. Norris, R. Anderson, and I. C. Kenny, “Method analysis of accelerometers and gyroscopes in running gait: A systematic review,” *Proc. Inst. Mech. Eng. Part P J. Sports Eng. Technol.*, vol. 228, no. 1, pp. 3–15, Mar. 2014.
[23] D. Steins, I. Sheret, H. Dawes, P. Esser, and J. Collett, “A smart device inertial-sensing method for gait analysis,” *J. Biomech.*, vol. 47, no. 15, pp. 3780–3785, Nov. 2014.
[24] J. Taborri, S. Rossi, E. Palermo, F. Patanè, and P. Cappa, “A novel HMM distributed classifier for the detection of gait phases by means of a wearable inertial sensor network,” *Sensors*, vol. 14, no. 9, pp. 16212–16234, Sep. 2014.
[25] J. C. Handsaker, S. E. Forrester, J. P. Folland, M. I. Black, and S. J. Allen, “A kinematic algorithm to identify gait events during running at different speeds and with different footstrike types,” *J. Biomech.*, vol. 49, no. 16, pp. 4128–4133, 08 2016.
[26] J. Leitch, J. Stebbins, G. Paolini, and A. B. Zavatsky, “Identifying gait events without a force plate during running: A comparison of methods,” *Gait Posture*, vol. 33, no. 1, pp. 130–132, Jan. 2011.
[27] T. Seel, J. Raisch, and T. Schauer, “IMU-Based Joint Angle Measurement for Gait Analysis,” *Sensors*, vol. 14, no. 4, pp. 6891–6909, Apr. 2014.
[28] E. M. Debbi *et al.*, “In-shoe center of pressure: indirect force plate vs. direct insole measurement,” *Foot*, vol. 22, no. 4, pp. 269–275, Dec. 2012.
[29] M. Koch, L.-K. Lunde, M. Ernst, S. Knardahl, and K. B. Veiersted, “Validity and reliability of pressure-measurement insoles for vertical ground reaction force assessment in field situations,” *Appl. Ergon.*, vol. 53 Pt A, pp. 44–51, Mar. 2016.
[30] S. Barnett, J. L. Cunningham, and S. West, “A comparison of vertical force and temporal parameters produced by an in-shoe pressure measuring system and a force platform,” *Clin. Biomech.*, vol. 16, no. 4, pp. 353–357, May 2001.
[31] D. C. Low and S. J. Dixon, “Footscan pressure insoles: accuracy and reliability of force and pressure measurements in running,” *Gait Posture*, vol. 32, no. 4, pp. 664–666, Oct. 2010.
[32] S. Crea, M. Donati, S. M. M. De Rossi, C. M. Oddo, and N. Vitiello, “A Wireless Flexible Sensorized Insole for Gait Analysis,” *Sensors*, vol. 14, no. 1, pp. 1073–1093, Jan. 2014.
[33] T. Stöggl and A. Martiner, “Validation of Moticon’s OpenGo sensor insoles during gait, jumps, balance and cross-country skiing specific imitation movements,” *J. Sports Sci.*, vol. 35, no. 2, pp. 196–206, Jan. 2017.
[34] F. T. Price, “Validation of a Wearable Sensor Insole Device for Analysis of Postural Control,” Miami University, 2018.
[35] “Moticon_Insole-Instruction-Manual_1.2.” Moticon.

[36] “NV08C-RTK.” [Online]. Available: http://www.nvs-gnss.com/products/receivers/item/39-nv08c-rtk.html. [Accessed: 06-Apr-2019].
[37] “VN-200 - VectorNav Technologies.” [Online]. Available: https://www.vectornav.com/products/vn-200. [Accessed: 05-Apr-2019].
[38] G. Falco, M. Pini, and G. Marucco, “Loose and Tight GNSS/INS Integrations: Comparison of Performance Assessed in Real Urban Scenarios,” *Sensors*, vol. 17, no. 2, Jan. 2017.
[39] H. Tan, A. M. Wilson, and J. Lowe, “Measurement of stride parameters using a wearable GPS and inertial measurement unit,” *J. Biomech.*, vol. 41, no. 7, pp. 1398–1406, 2008.
[40] S. Bichler, G. Ogris, V. Kremser, F. Schwab, S. Knott, and A. Baca, “Towards high-precision IMU/GPS-based stride-parameter determination in an outdoor runners’ scenario,” *Procedia Eng.*, vol. 34, pp. 592–597, Jan. 2012.
[41] J. Merritt, “Learning to Fly: Decrease Ground Contact Time | Metric Series #3,” *MilestonePod*. [Online]. Available: https://www.milestonepod.com/jackies_journey/learning-to-fly-decrease-ground-contact-time/. [Accessed: 05-Apr-2019].
[42] T. S. Keller, A. M. Weisberger, J. L. Ray, S. S. Hasan, R. G. Shiavi, and D. M. Spengler, “Relationship between vertical ground reaction force and speed during walking, slow jogging, and running,” *Clin. Biomech.*, vol. 11, no. 5, pp. 253–259, Jul. 1996.
[43] R. Tanawongsuwan and A. Bobick, *A Study of Human Gaits across Different Speeds*. Georgia Tech: Tech. Rep, 2003.
[44] A. Tongen and R. E. Wunderlich, “Biomechanics of Running and Walking,” *Mathematics and Sports*, Aug-2010. [Online]. Available: /core/books/mathematics-and-sports/biomechanics-of-running-and-walking/0DC334F72A56527FC4517B297923E9D3. [Accessed: 05-Apr-2019].
[45] K. J.-H. Ngoh, D. Gouwanda, A. A. Gopalai, and Y. Z. Chong, “Estimation of vertical ground reaction force during running using neural network model and uniaxial accelerometer,” *J. Biomech.*, vol. 76, pp. 269–273, 2018.
[46] R. D. Gurchiek, R. S. McGinnis, A. R. Needle, J. M. McBride, and H. van Werkhoven, “The use of a single inertial sensor to estimate 3-dimensional ground reaction force during accelerative running tasks,” *J. Biomech.*, vol. 61, pp. 263–268, 2017.
[47] S. Gaglani, J. Moore, M. R. Haynes, J. B. Hoffberger, and D. Rigamonti, “Using Commercial Activity Monitors to Measure Gait in Patients with Suspected iNPH: Implications for Ambulatory Monitoring,” *Cureus*, vol. 7, no. 11.
[48] J. M. Bock, L. A. Kaminsky, M. Harber, and A. H. K. Montoye, “Determining the Reliability of Several Consumer-Based Physical Activity Monitors,” 2017, vol. 5, p. 3.
[49] Garmin and G. L. or its subsidiaries, “HRM-Run™,” *Garmin*. [Online]. Available: https://buy.garmin.com/fi-FI/FI/p/530376. [Accessed: 04-Apr-2019].
[50] A. Ignatov, “Real-time human activity recognition from accelerometer data using Convolutional Neural Networks,” *Appl. Soft Comput.*, vol. 62, pp. 915–922, Jan. 2018.
[51] F. J. Wouda *et al.*, “Estimation of Vertical Ground Reaction Forces and Sagittal Knee Kinematics During Running Using Three Inertial Sensors,” *Front. Physiol.*, vol. 9, p. 218, 2018.
[52] S. E. Oh, A. Choi, and J. H. Mun, “Prediction of ground reaction forces during gait based on kinematics and a neural network model,” *J. Biomech.*, vol. 46, no. 14, pp. 2372–2380, Sep. 2013.
[53] N. Nazmi, M. A. Abdul Rahman, S.-I. Yamamoto, and S. A. Ahmad, “Walking gait event detection based on electromyography signals using artificial neural network,” *Biomed. Signal Process. Control*, vol. 47, pp. 334–343, Jan. 2019.

[54] H. T. T. Vu, F. Gomez, P. Cherelle, D. Lefeber, A. Nowé, and B. Vanderborght, “ED-FNN: A New Deep Learning Algorithm to Detect Percentage of the Gait Cycle for Powered Prostheses,” in *Sensors*, 2018, vol. 18, p. 2389.
[55] P. Davidson, H. Virekunnas, D. Sharma, R. Piché, and N. Cronin, “Continuous Analysis of Running Mechanics by Means of an Integrated INS/GPS Device,” *Sensors*, vol. 19, no. 6, p. 1480, Jan. 2019.
[56] “Stance Phase - an overview | ScienceDirect Topics.” [Online]. Available: https://www.sciencedirect.com/topics/engineering/stance-phase. [Accessed: 11-Apr-2019].
[57] “Biomechanics of Walking,” *FootEducation*. [Online]. Available: https://footeducation.com/biomechanics-of-walking-gait/. [Accessed: 11-Apr-2019].
[58] J. Taborri, E. Palermo, S. Rossi, and P. Cappa, “Gait Partitioning Methods: A Systematic Review,” *Sensors*, vol. 16, no. 1, Jan. 2016.
[59] J. Carpentier, M. Benallegue, and J.-P. Laumond, “On the centre of mass motion in human walking,” *Int. J. Autom. Comput.*, vol. 14, no. 5, pp. 542–551, Oct. 2017.
[60] “(PDF) Normal gait,” *ResearchGate*. [Online]. Available: https://www.researchgate.net/publication/297048967_Normal_gait. [Accessed: 12-Apr-2019].
[61] G. Carlet, *Essai expérimental sur la locomotion humaine : Etude de la marche*. Paris: E. Martinet, 1872.
[62] A. Guiotto, A. Scarton, Z. Sawacha, G. Guarneri, A. Avogaro, and C. Cobelli, “Gait analysis driven 2d finite element model of the neuropathic hindfoot,” *J. Mech. Med. Biol.*, vol. 16, no. 02, p. 1650012, Mar. 2015.
[63] L. Breiman, J. H. Friedman, R. A. Olshen, and C. J. Stone, “Review of Classification and Regression Trees,” *Biometrics*, vol. 40, no. 3, pp. 874–874, 1984.
[64] T. J. Hastie, *Generalized additive models*. Chapman and Hall, 1990.
[65] “Luís Torgo - PhD Thesis.” [Online]. Available: http://www.dcc.fc.up.pt/~ltorgo/PhD/. [Accessed: 03-Jul-2019].
[66] L. Breiman, “Bagging Predictors,” *Mach. Learn.*, vol. 24, no. 2, pp. 123–140, Aug. 1996.
[67] “Create bag of decision trees - MATLAB - MathWorks Nordic.” [Online]. Available: https://se.mathworks.com/help/stats/treebagger.html. [Accessed: 04-Jul-2019].
[68] “1.6. Nearest Neighbors — scikit-learn 0.20.3 documentation.” [Online]. Available: https://scikit-learn.org/stable/modules/neighbors.html#regression. [Accessed: 15-Apr-2019].
[69] J. Brownlee, “Making Predictions with Sequences,” *Machine Learning Mastery*, 03-Sep-2017. [Online]. Available: https://machinelearningmastery.com/sequence-prediction/. [Accessed: 15-Apr-2019].
[70] R. Sun and C. L. Giles, “Sequence learning: from recognition and prediction to sequential decision making,” *IEEE Intell. Syst.*, vol. 16, no. 4, pp. 67–70, Jul. 2001.
[71] J. Fan, C. Ma, and Y. Zhong, “A Selective Overview of Deep Learning,” *ArXiv190405526 Cs Math Stat*, Apr. 2019.
[72] “Quaternion Math.” VECTORNAV.
[73] “Trapezoidal numerical integration - MATLAB trapz - MathWorks Nordic.” [Online]. Available: https://se.mathworks.com/help/matlab/ref/trapz.html. [Accessed: 26-Apr-2019].
[74] “Moticon-ORTHO_booklet_en_print_01.01.02.” Moticon.
[75] “Keras,” 2015. [Online]. Available: https://keras.io/. [Accessed: 18-Aug-2019].